https://doi.org/10.59761/RCR5124

Heterostructures based on g-C_3N_4 for the photocatalytic CO_2 reduction

Roman F. Alekseev,[a,b] Andrey A. Saraev,[a] Anna Yu. Kurenkova,[a] Ekaterina A. Kozlova[a]

[a] *Boreskov Institute of Catalysis, Siberian Branch of the Russian Academy of Sciences, prosp. Akademika Lavrentieva 5, 630090 Novosibirsk, Russian Federation*
[b] *Novosibirsk State University, ul. Pirogova 2, 630090 Novosibirsk, Russian Federation*

The interest of the global scientific community in the problems of CO_2 utilization and returning to the carbon cycle has markedly increased in recent years. Among various CO_2 transformation processes, photocatalytic reduction is one of the most promising. Currently, much attention is paid to photocatalysts based on graphitic carbon nitride, since the use of g-C_3N_4 makes it possible to perform CO_2 reduction under visible or solar light irradiation. To increase the reduction efficiency, g-C_3N_4 is subjected to various modifications with the most popular and promising approach being the synthesis of composite photocatalysts based on g-C_3N_4 with other semiconductors to form heterostructures. Depending on the type of semiconductor, transfer of photogenerated charge carriers in these systems can occur by various mechanisms, which largely determine the course of the process and the rates of formation of reaction products. This review addresses studies on the synthesis of composite photocatalysts based on g-C_3N_4, with emphasis being placed on the mechanisms of charge carrier transfer and the distribution of products of CO_2 reduction.
The bibliography includes 235 references.

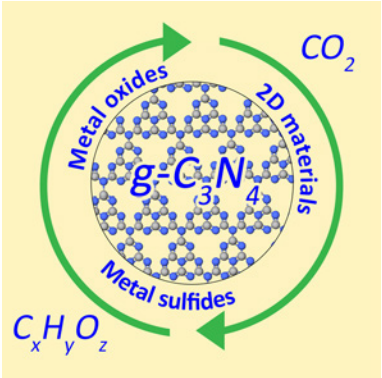

Keywords: photocatalysis; photocatalyst; heterogeneous catalysis; graphitic carbon nitride; carbon dioxide reduction; charge carrier separation mechanism; heterostructures; solar energy.

Contents

1. Introduction

A primary task of rational management and protection of the environment is to reduce the concentration and emissions of greenhouse gases. The development of methods for reducing concentrations of greenhouse gases is the subject of many studies,[1–3] with much attention being paid to utilization of carbon dioxide, the major component of greenhouse gases.[4–8]

Today, there are several industrial processes for converting CO_2 to valuable products such as urea, salicylic acid, ethylene carbonate and methanol. Due to the high thermodynamic stability of the CO_2 molecule, traditional processes of CO_2 conversion to products are carried out at high temperature and high pressure, *e.g.*, synthesis of urea from CO_2 and NH_3 takes plates at a temperature of 185 °C and a pressure of 150 bar,[9–11] which substantially increases the energy expenditure and

R.F.Alekseev. Bachelor.
E-mail: r.alekseev@g.nsu.ru
Current research interests: photocatalytic CO_2 reduction, heterogeneous photocatalysts.
A.A.Saraev. PhD in Physics and Mathematics, Senior Researcher.
E-mail: asaraev@catalysis.ru
Current research interests: heterogeneous catalysis and photocatalysis, X-ray and spectroscopic methods.
A.Yu.Kurenkova. PhD in Chemistry, Senior Researcher.
E-mail: kurenkova@catalysis.ru
Current research interests: photocatalytic processes and heterogeneous photocatalysts for H_2 production and CO_2 reduction.
E.A.Kozlova. Doctor of Chemical Sciences, Professor of RAS, Leading Researcher. E-mail: kozlova@catalysis.ru
Current research interests: semiconductor photocatalysis for alternative energy production processes, heterogeneous photocatalysts for H_2 production, CO_2 reduction and degradation of organic pollutants.

Translation: Z.P.Svitanko

Received 26 March 2024

decreases the economic attractiveness of these processes, despite the readily available feedstock.

For this reason, of particular interest are the ways to decrease the energy consumption of CO_2 conversion processes. One of the approaches to address this task is the photocatalytic reduction of CO_2, which can occur under ambient conditions.[7,12] This process is based on the use of renewable resources, solar light and water, which makes photocatalytic reduction a promising method for CO_2 utilization, but its industrial implementation is primarily limited by the lack of efficient photocatalysts. Nevertheless, photocatalytic reduction of CO_2 complies with the principles of sustainable development and, in the future, it may become the most facile and inexpensive way for decreasing the CO_2 concentration in the atmosphere.[12,13] Moreover, this process gives organic compounds such as CH_4, CH_3OH and HCOOH [equations (1)–(5), standard electrode potentials *vs.* NHE at pH = 7 are given], which can be used as synthetic fuel and in chemical industy.[12,14–17]

$$CO_2 + 2H^+ + 2e^- \longrightarrow HCOOH,\ E^0 = -0.66\ V \quad (1)$$

$$CO_2 + 2H^+ + 2e^- \longrightarrow CO + H_2O,\ E^0 = -0.52\ V \quad (2)$$

$$CO_2 + 4H^+ + 4e^- \longrightarrow CH_2O + H_2O,\ E^0 = -0.49\ V \quad (3)$$

$$CO_2 + 6H^+ + 6e^- \longrightarrow CH_3OH + H_2O,\ E^0 = -0.40\ V \quad (4)$$

$$CO_2 + 8H^+ + 8e^- \longrightarrow CH_4 + 2H_2O,\ E^0 = -0.25\ V \quad (5)$$

In recent years, the attention of researchers has been attracted to a new polymer semiconductor, graphitic carbon nitride g-C_3N_4 (Fig. 1), materials based on which can be used in various photocatalytic reactions.[18,19] It is found that g-C_3N_4 has a planar structure based on heptazine or triazine units,[20] in which carbon and nitrogen atoms are sp^2-hybridized. This promising semiconductor has high chemical and thermal stability; in addition, g-C_3N_4 can be obtained from readily available precursors by simple methods.[21,22] As compared with many semiconductors traditionally used in photocatalysis, for example TiO_2, g-C_3N_4 has a rather narrow band gap (2.7 eV); in combination with the highly negative position of the conduction band (–1.3 V *vs.* NHE), this results in light absorption over a broad range of wavelengths and a high reduction potential of photogenerated electrons.[23,24] In addition, g-C_3N_4 has a number of properties inherent in two-dimensional materials such as high mobility of charge carriers, high surface area to volume ratio and the presence of quantum size effect.[25,26] The drawbacks of g-C_3N_4 include fast recombination of photoinduced electron–hole pairs [27] and low adsorption ability, which hampers any heterogeneous catalytic process.[28,29] A popular and efficient approach to overcome these difficulties is to form heterostructures with other semiconductors or materials, which would enhance the efficiency of charge carrier separation and the adsorption properties.

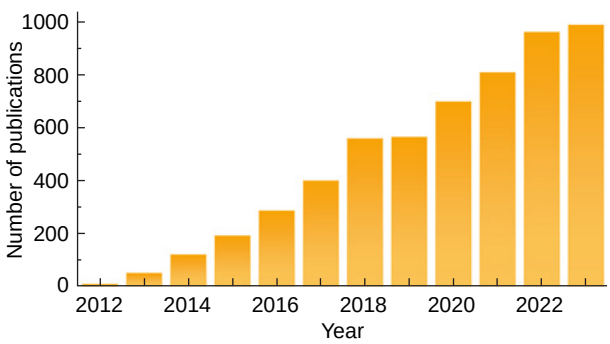

Figure 1. Number of publications dealing with g-C_3N_4-based photocatalysts in recent years according to the Scopus database.

It is known that photocatalysts are activated upon absorption of light quanta with energy equal to or exceeding the size of the band gap energy of the semiconductor. As this takes place, the electron migrates from the valence band to the conduction band, and an electron vacancy (hole) appears in the conduction band. Then the photogenerated electrons and holes can either migrate to the photocatalyst surface and be involved in redox reactions with adsorbed reagents or recombine in the photocatalyst bulk to release heat. The recombination of electron–hole pairs sharply decreases the efficiency of the photocatalytic reaction; therefore, an important task of photocatalysis is separation of the photogenerated charge carriers to increase their lifetime.

On contact of two semiconductors, the difference between the Fermi levels induces the electron transfer, giving rise to a built-in electric field, which, in turn, promotes the transfer of photoinduced charge carriers.[30–32] The charge carrier separation in composite structures can proceed by different mechanisms. The classical schemes of charge carrier transfer between two semiconductors include type I and II heterojunctions. Type I heterojunction appears when the conduction band (CB) of one semiconductor (SC 2 in Fig. 2*a*) is located lower, while its valence band (VB) is located higher in energy than these bands of another semiconductor (SC 1 in Fig. 2*a*). In such a structure, electrons and holes would migrate from the wide-band-gap semiconductor to the narrow-band-gap one and be accumulated in one semiconductor and subsequently recombine. In type II heterojunction, both the valence and conduction bands of one semiconductor are higher in energy than those of another semiconductor, and the transfer of electrons from a semiconductor with higher conduction band level (SC 1 in Fig. 2*b*) to a semiconductor with lower conduction band level (SC 2 in Fig. 2*b*) is formed, while holes migrate from lower valence band in SC 2 to higher valence band in SC 1 (Fig. 2*b*). In this case, electrons and holes are accumulated in different semiconductors, and their lifetime is thus increased.

As a rule, charge carrier separation mechanisms in composite photocatalysts composed of g-C_3N_4 and another semiconductor are based on type II heterojunction or direct Z-scheme. Later, S-scheme heterojunction was proposed.[33] The direct Z-scheme transfer mechanism occurs between two semiconductors the energy structure of which is similar to that described above for type II heterojunction. However, in this case, an electron with a low reduction potential (in SC 2) recombines with a hole that has a low oxidation potential (in SC 1); in comparison with type II heterojunction, this gives rise to charge carriers with a higher redox potential. The separation of charge carriers between two semiconductors according to the S-scheme is similar to the direct Z-scheme; however, the S-scheme takes into account the semiconductor band bending caused by alignment of their Fermi levels and generation of the built-in electric field in the photocatalyst.[34] As a rule, Z-scheme is implemented by two n-type and p-type semiconductors, while S-scheme is implemented by n-type semiconductors, considered as an oxidation photocatalyst and reduction photocatalyst (see Fig. 2).[3,35,36] Both Z-scheme and S-scheme can be either direct (Fig. 2*d*) or indirect (Fig. 2*e*); in the latter case, compounds with high electrical conductivity, *e.g.*, metals or some carbon materials such as graphene, serve as mediators.[37] It is important that implementation of either Z- or S-scheme in a composite

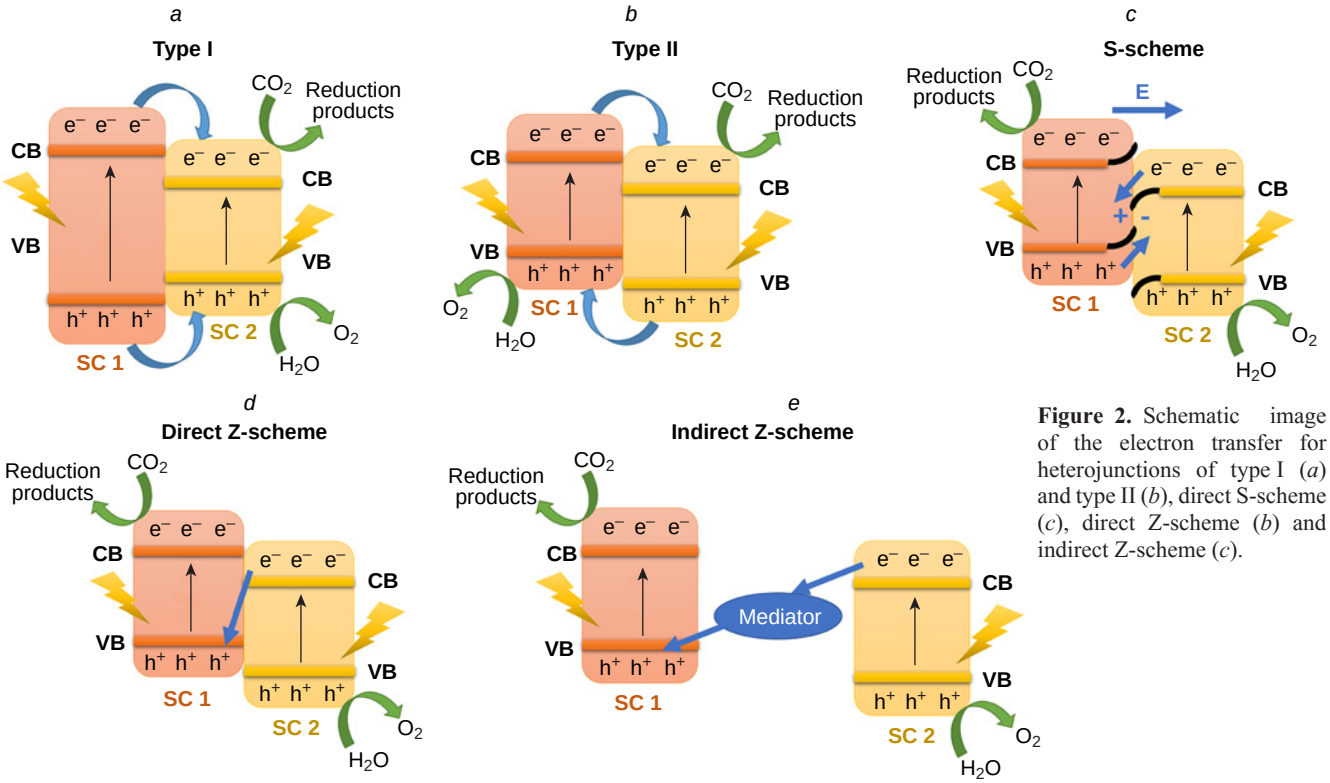

Figure 2. Schematic image of the electron transfer for heterojunctions of type I (*a*) and type II (*b*), direct S-scheme (*c*), direct Z-scheme (*b*) and indirect Z-scheme (*c*).

photocatalyst not only increases the efficiency of separation of the electron–hole pairs, but also maximizes the redox capacity of charge carriers.

One more popular method for increasing the lifetime of photogenerated charge carriers is deposition of metals on the semiconductor surface. The Schottky junction is formed at the metal-semiconductor interface, and electrons from the conduction band of the semiconductor move to Fermi level of metal, which leads to alignment of the metal and semiconductor Fermi levels and bending of semiconductor bands near the interface.

Apart from the lifetime of photogenerated charge carriers, another important characteristic of semiconductor photocatalysts is the size of the optical band gap (below referred to as band gap), which determines the minimum energy of light quantum necessary for generation of electron–hole pairs (Fig. 3).[38] As a rule, the band gap energy is derived from the diffuse reflectance spectroscopy by the method proposed by Jan Tauc.[39] First, the absorption coefficient F(R) is found using the Kubelka–Munk equation:

$$F(R) = \frac{(1-R)^2}{2R} \qquad (6)$$

where R is the reflection factor of the sample determined from the diffuse reflectance spectroscopy data.

Using the Tauc equation, the dependence of the absorption coefficient F(R) on the photon energy is found:

$$(F(R)\,h\nu)^{1/\gamma} = B(h\nu - E_g) \qquad (7)$$

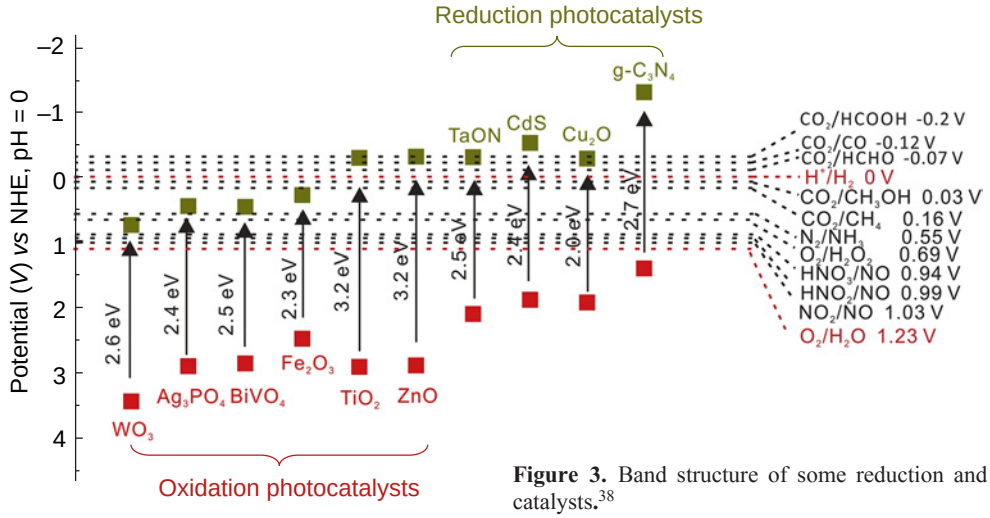

Figure 3. Band structure of some reduction and oxidation photocatalysts.[38]

where h is the Planck constant, ν is the photon frequency, E_g is the band gap energy, B is a constant, γ is the factor equal to 1/2 for direct junctions and to 2 for indirect junctions.

The intersection of the tangent to the Tauc plot with the abscissa gives the band gap energy of the semiconductor. It is noteworthy that this method is suitable for determining the band gap energy of unmodified semiconductors. Determining the band gap energy for composite materials, especially in the case of different types of electron transfer (direct/indirect) in semiconductors gives, most often, incorrect results. Nevertheless, in many publications, analysis of band gap changes based on diffuse reflectance spectroscopy is often performed for composite materials. In this case, the spectrum of the photocatalyst is usually a linear combination of the spectra of independet components, except the cases where quantum size effects or localized surface plasmon resonance influence the optical properties of materials. In some cases, the band gap of modified semiconductors can be estimated by drawing the tangent to the region called Urbach tail in the diffuse reflectance spectra. Then the intersection of this tangent with the tangent to the Tauc plot gives a correct band gap energy for a single component of a photocatalyst.[40]

It is known that graphitic carbon nitride can behave as either p-type or n-type semiconductor depending on the external effects such as the applied voltage and redox potential of a reagent.[41–45] For example, g-C_3N_4 behaves as a p-type semiconductor when a negative voltage is applied and as an n-type semiconductor when the voltage is positive; therefore, it can be considered as an amphoteric semiconductor.[42,46,47] The amphoteric semiconductor properties also depend on the g-C_3N_4 bulk structure and surface functionalization.[48] Hence, the charge carrier transfer mechanism in composite photocatalysts composed of g-C_3N_4 and a semiconductor with a high potential of photogenerated holes can be considered as a Z-scheme or S-scheme, as described below.

Traditionally, g-C_3N_4 is obtained by heat treatment of various nitrogen-containing precursors such as melamine, dicyandiamide, and urea,[49–51] but, most often, this method does not provide a material with a high specific surface area. In recent years, numerous new approaches to the synthesis of g-C_3N_4 have been proposed providing the possibility of varying the particle size, pore volume and specific surface area of the resulting material.[52] The methods of synthesis of g-C_3N_4 are comprehensively addressed in the literature;[22,53–57] therefore, they are not discussed here.

This review is focused on g-C_3N_4 heterostructures with other materials used for photocatalytic CO_2 reduction. It is noteworthy that there are a few published reviews dealing with modification of g-C_3N_4 and fabrication of heterostructures for the photocatalytic reduction of CO_2 [58–64] considering photocatalysts in the light of charge carrier transfer mechanisms or the effect of methods of synthesis on the photocatalytic properties. There are also reviews on using g-C_3N_4-based systems for other photocatalytic reactions (hydrogen evolution, decomposition of dyes, water treatment, *etc.*).[54,65,66] A widely used photocatalyst is g-C_3N_4 with platinum deposited on its surface, which is obtained by photoreduction of H_2PtCl_6 in a solution of an electron donor, most often, triethanolamine or by reduction with a solution of $NaBH_4$.[67,68] Modification of semiconductors with transition metals to enhance the photocatalytic activity has also been studied in detail and presented in the literature.[69–71]

This review is devoted to the most recent advances in the field of g-C_3N_4-based heterostructures for photocatalytic CO_2 reduction. The attention is focused on the materials used and the most likely mechanism of charge carrier transfer between the semiconductors. In addition, a distinctive feature of this review is comparison of the photocatalyst activity in terms of the overall rate of consumption of photogenerated electrons, which makes it possible to compare the activities of photocatalysts with different selectivities to CO_2 reduction products. The review addresses the most widely used and promising systems containing metal oxides and sulfides, two-dimensional metal carbides (MXenes) and carbon materials. Since in some cases the literature provides information about different possible heterojunctions for the same type of heterostructure, the role of the type of charge carrier separation mechanism is also analyzed in each Section.

2. g-C_3N_4-based heterostructures with metal oxides

2.1. Heterostructures with titanium dioxide

Titanium dioxide is one of the most popular photocatalysts used both for CO_2 reduction and for other photocatalytic processes, which is due to the low cost, stability and low toxicity of TiO_2.[72–74] However, the use of TiO_2-based photocatalysts is limited by the large band gap (~3.2 eV), since only UV photons have sufficient energy to induce the photoexcitation in TiO_2.[12,75] As a consequence, TiO_2 has low activity under the sunlight, in which the fraction of ultraviolet radiation is much smaller than that of the visible radiation. To increase the response of TiO_2-based photocatalysts to visible light, TiO_2 is modified with narrow-band-gap semiconductors, for example, g-C_3N_4.[76]

Titanium dioxide is known to have three stable crystalline phases — anatase, rutile, and brookite (Fig. 4).[21,77–79] As a rule, the first two of them are used in photocatalytic studies; anatase is considered to be more active than rutile, because of the higher reduction potential of electrons and the ability to form hole traps,[80,81] which is attributable to different predominant orientations of the crystallite surfaces in rutile and anatase. In the case of anatase, the crystallite surface is enriched with {101} and {001} faces, while in the case of rutile, {110}, {100} and {101} faces predominate.[82] It is known that the {001} face is more reactive in photocatalytic reactions.[83,84] Meanwhile, rutile has a narrower band gap than anatase and, hence, it can be used for reactions under irradiation at longer wavelengths.[85] The

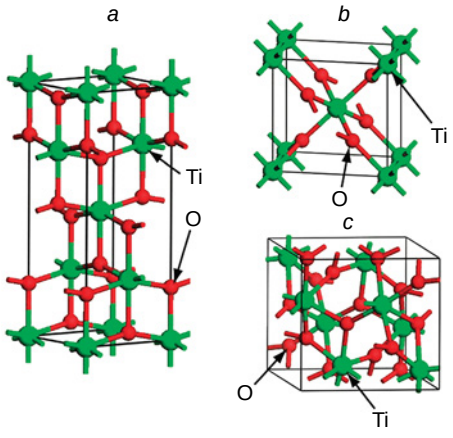

Figure 4. Crystal structure of TiO_2 phases: (*a*) anatase, (*b*) rutile, (*c*) brookite.[79] Published with permission from the Royal Society of Chemistry.

conduction band minimum in TiO_2 is approximately –0.2 V (*vs.* NHE at pH = 7),[21] which is insufficient for CO_2 reduction, since the formation potential of most products is more negative [see Eqns (1)–(5)]. However, the conduction band minimum in g-C_3N_4 is approximately –1.20 V (*vs* NHE at pH = 7), which is sufficient for the formation of various organic compounds from CO_2.[21]

In the formation of g-C_3N_4-based composite photocatalysts, the particles of other components are usually distributed over the g-C_3N_4 surface, because it has a layered structure where the longitudinal particle size substantially exceeds the transverse size. These composite structures are commonly designated by X/g-C_3N_4 (X is a component of a g-C_3N_4-based photocatalyst), *e.g.*, TiO_2/g-C_3N_4. This notation is used in this review, although authors of original publications may use other designations for heterostructures.

A fairly widespread method for the synthesis of TiO_2/g-C_3N_4 composites is physical mixing of components, according to which the components (TiO_2 and g-C_3N_4) are synthesized separately.[19,86] TiO_2 is obtained, most often, by hydrolysis, hydrothermal or solvothermal treatment of titanium-containing precursors such as titanium alkoxides.[19,73]

Mehregan *et al.*[87] proposed a method for the fabrication of TiO_2/g-C_3N_4 composite by hydrothermal treatment [hereinafter, slash (/) is used in the designations of heterostructures, while a hyphen (–) designates semiconductors doped with metal or non-metal atoms]. Titanium dioxide was prepared by the sol–gel method using titanium tetrabutoxide as the precursor, while g-C_3N_4 was obtained by melamine calcination followed by exfoliation to give a layered structure (Fig. 5). A suspension consisting of weighed portions of TiO_2 and g-C_3N_4 obtained in this way (in 2 : 1 w/w ratio of TiO_2 to g-C_3N_4) and aqueous ethanol was sonicated and then placed in an autoclave and kept at 120 °C for 3 h. The CO_2 reduction was carried out in the gas phase in the presence of water vapour on exposure to visible light. The authors studied the effect of light intensity on the reaction rate and showed a pronounced increase in the photocatalyst activity with as the light power density increased from 20 to 80 mW cm^{-2}. Thus, the light intensity of 80 mW cm^{-2} provided the highest product formation rates, 33 and 1.4 μmol g^{-1} h^{-1} for CH_4 and CH_3OH, respectively. In some other publications, it is also shown that increase in the light power density increases the rates of electron and hole generation, which results in a higher photocatalyst activity.[88,89]

It should be emphasized that Evonik P25, a commercial TiO_2 powder, is used most often for the synthesis of various TiO_2-based photocatalysts.[12] This TiO_2 powder is composed of 80% anatase and 20% rutile with an average particle size of 25 nm and has a specific surface area of 40–60 m^2 g^{-1}.[90] Wang *et al.*[91] synthesized TiO_2/g-C_3N_4 composite photocatalysts with various component ratios by ball milling of TiO_2 (anatase) with g-C_3N_4 pretreated with a solution of HNO_3 to form a layered structure (Fig. 6). Then the mixture was calcined at 400 °C for 1 h to form the composite material with TiO_2 particles deposited on the g-C_3N_4 surface. The authors demonstrated a change in the positions of the valence and conduction bands depending on the component ratio and increase in the band gap with increasing TiO_2 content. This study describes the liquid-phase CO_2 reduction in which the suspension with a photocatalyst in aqueous NaOH and triethanolamine solution was placed in a reactor, and then purged with CO_2 flow. The highest activity after 4 h of UV irradiation (8 W lamp) was found for the photocatalyst with TiO_2 to g-C_3N_4 ratio of 1 : 2. The rates of CO and CH_4 formation were 14 and 18 μmol g^{-1} h^{-1}, respectively, which was twice as high as that for pristine g-C_3N_4.

Truc *et al.*[92] synthesized composite photocatalysts based on g-C_3N_4 and niobium-doped TiO_2 in which the direct Z-scheme heterojunction was formed (Fig. 7).[92] The introduction of Nb into TiO_2 structure leads to the formation of Ti^{3+} ions and the appearance of an additional energy level near the TiO_2 conduction band, thus reducing the band gap size from 3.2 to 2.9 eV. The change in the band gap by introducing metal and non-metal ions into a parent substance is a common method used to shift the absorption edge of photocatalysts.[93–97] The

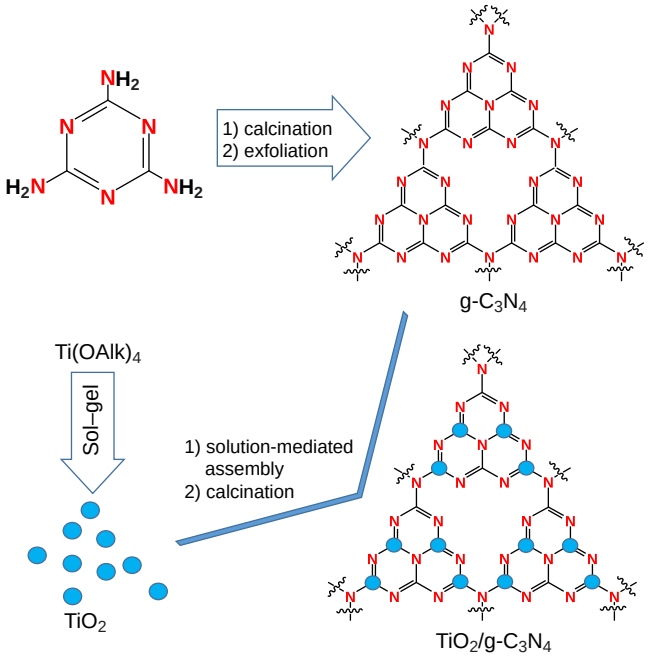

Figure 5. Schematic diagram of the approach to the fabrication of TiO_2/g-C_3N_4 heterostructures.

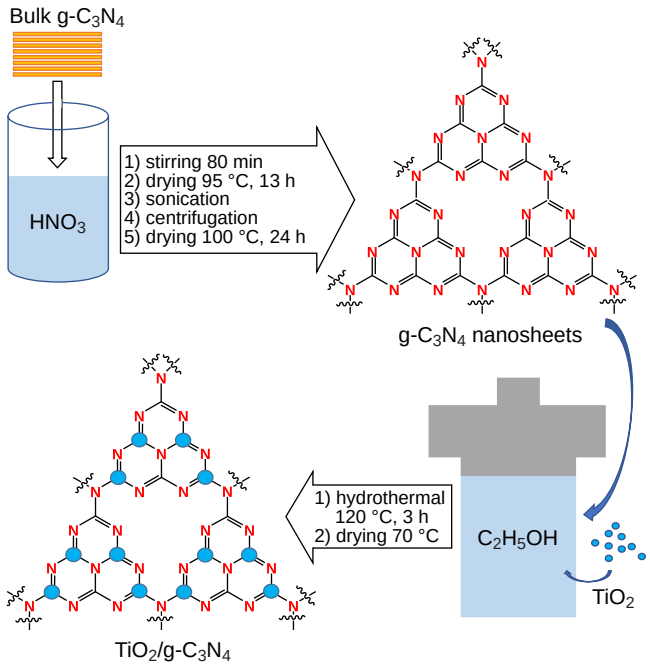

Figure 6. Schematic diagram of the synthesis of the TiO_2/g-C_3N_4 photocatalyst.[91]

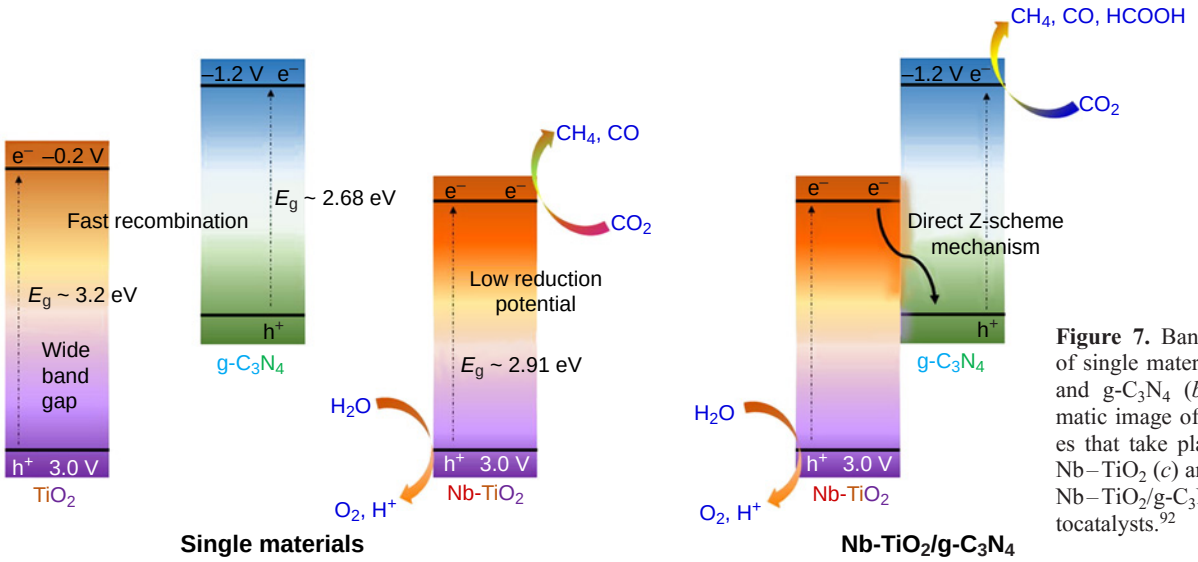

Figure 7. Band structure of single materials TiO_2 (*a*) and g-C_3N_4 (*b*) and schematic image of the processes that take place in doped Nb–TiO_2 (*c*) and composite Nb–TiO_2/g-C_3N_4 (*d*) photocatalysts.[92]

Nb–TiO_2/g-C_3N_4 composite photocatalysts were obtained by calcination of a mixture of Nb–TiO_2 with melamine. In a series of experiments on the gas-phase photocatalytic CO_2 reduction on exposure to light from two 30-W white lamps, the highest activity was detected for the photocatalyst with 1 : 1 ratio of (Nb–TiO_2) to g-C_3N_4. Apart from CO and CH_4, the reaction products were found to contain formic acid and oxygen resulting from water oxidation. The formation rates of CO, CH_4, HCOOH and O_2 were 420, 560, 700 and 1700 μmol g^{-1} h^{-1}, respectively. The results obtained in this work demonstrate the high potential of the integrated approach to the synthesis of photocatalysts, including both doping and the formation of heterojunctions in composite materials.

To compare the activity of photocatalysts with different selectivities to reaction products, it was proposed to use the total number of electrons absorbed in the photocatalytic process per unit time and per unit mass of the photocatalyst, W_e, which is calculated by the equation:[98]

$$W_e = 2\,W_{CO} + 8\,W_{CH_4} + 6\,W_{CH_3OH} + 2\,W_{HCOOH} \qquad (8)$$

where W_{CO}, W_{CH_4}, W_{CH_3OH}, and W_{HCOOH} are the rates of formation of the products per unit mass of the photocatalyst (as a rule, μmol g^{-1} h^{-1}); coefficients are determined by the number of electrons needed for the formation of this product. Methane makes the greatest contribution to W_e, because its formation requires more electrons than the formation of other compounds [see Eqns (1)–(5)]. Equation (8) or similar relations are convenient for calculating the apparent quantum efficiency (AQE) [Equation (9)] and are widely used in the studies of the photocatalytic CO_2 reduction, although the terminology may differ.[7,98–101]

$$\mathrm{AQE} = \frac{W_e^*}{N_{ph}} \times 100\% \qquad (9)$$

where W_e* is the product formation rate with allowance for the electron balance (usually μmol h^{-1}), N_{ph} is the photon flux from the light source calculated from the data on the irradiation power and spectrum (μmol h^{-1}).

Unfortunately, AQE values for the photocatalytic CO_2 reduction (usually not exceeding 1%) are rarely reported in the literature; therefore, comparison of the photocatalyst activity will be based on calculation of the rate W_e.[12] However, it is noteworthy that AQE is an important characteristic of photocatalytic systems, as it reflects the photon utilization efficiency, while the rate W_e depends, among other factors, on the light irradiation power. The only outstanding AQE value was repotrted by Zhang *et al.*[102] A composite photocatalyst based on g-C_3N_4 and Ag-doped TiO_2 has an AQE of 2.4% in the liquid-phase CO_2 reduction. It is shown that the addition of Ag promotes implementation of S-scheme heterojunctions and electron transfer from TiO_2 to g-C_3N_4. In addition, high efficiency of CO_2 reduction is attained owing to high specific surface area and defects in the g-C_3N_4 structure.

The data on TiO_2/g-C_3N_4 composite systems that were reported in recent years are summarized in Table 1, which also indicates the reaction conditions and reagents added to the reactor. To carry out the photocatalytic reaction, a flow of ultrapure CO_2 is usually purged through the reactor; however, the CO_2 generation directly in the reactor, *e.g.*, by the reaction of $NaHCO_3$ and H_2SO_4, can also be used. Most often, the source of protons in photocatalytic CO_2 reduction is water, but CH_4 can also serve for this purpose. Generally, TiO_2 is one of the most popular semiconductors for the synthesis of photocatalysts; therefore, there are numerous heterostructures based on TiO_2. A combination of TiO_2 with g-C_3N_4 in the TiO_2/g-C_3N_4 composite photocatalysts gives W_e values reaching 270 μmol g^{-1} h^{-1} under visible light irradiation,[87] while modification of the TiO_2/g-C_3N_4 composite leads to even a more pronounced increase in the activity. As can be seen from Table 1, high W_e value was attained for composite system comprising Z-scheme heterojunction and synthesized from TiO_2 doped with metal ions; therefore, this method appears to be most efficient.

2.2. Heterostructures with zinc oxide

Zinc oxide ZnO is widely used in various fields owing to its mechanical, electrical, optical and photocatalytic properties.[113,114] The most thermodynamically stable ZnO phase under ambient conditions is wurtzite (Fig. 8).[115,116] ZnO has a band gap of approximately 3.4 eV and n-type conduction, which makes it similar to TiO_2 for photocatalytic applications.[117] Hence, combination of ZnO with narrow-band-gap semiconductors such as g-C_3N_4 is also a promising approach for

Table 1. Review of some publications on CO_2 reduction in the presence of photocatalysts based on TiO_2/g-C_3N_4 (GP means that CO_2 reduction is carried out in the gas phase, while LP refers to liquid-phase reduction).

Photocatalyst	Light source	Conditions	Products, formation rates, μmol g^{-1} h^{-1}	W_e, μmol g^{-1} h^{-1}	Hetero-junction	Ref.
TiO_2/g-C_3N_4	300 W Xe lamp, 420 nm filter, 80 mW cm^{-2}	GP, CO_2+H_2O	CH_4, 32.5 CH_3OH, 1.44	269	Z-Scheme	87
TiO_2/g-C_3N_4	8 W UV lamp	LP, CO_2 + aqueous solution NaOH+TEOA	CO, 14.1 CH_4, 18.1	173	Type II	91
Nb–TiO_2/g-C_3N_4	Two 30 W white lamps	GP, CO_2 + H_2O	CO, 420 CH_4, 562 HCOOH, 698	6730	Z-Scheme	92
Ag/TiO_2/g-C_3N_4	300 W Xe lamp	GP, CO_2 + H_2O	CO, 17.3 CH_4, 35.4	318	Z-Scheme	102
g-C_3N_4@TiO_2 hollow spheres	300 W Xe lamp	LP, CO_2 + H_2O	CH_3OH, 8.68 CH_4, 3.55	80.5	Type II	103
Au/TiO_2@g-C_3N_4	300 W Xe lamp, 420 nm filter	GP, CO_2 + H_2O	CO, 21.7 CH_4, 37.4	343	Z-Scheme	104
TiO_2/g-C_3N_4	Solar simulator	GP, CO_2 + CH_4	CO, 9.98	20.0	Type II	105
TiO_2/g-C_3N_4 with C vacancies on the surface	Xe lamp, 420 nm filter, 210 mW cm^{-2}	GP, CO_2 + H_2O	CO, 0.974 CH_4, 0.05	2.35	Type II	106
Co^{2+}–TiO_2/g-C_3N_4	Xe lamp, 400 nm filter	LP, MeCN + TEOA + bpy + $CoCl_2$ in H_2O	CO, 287	574	Type II	107
TiO_2/g-C_3N_4/Ti_3C_2	350 W Xe lamp	GP, $NaHCO_3$ + H_2SO_4	CO, 4.39 CH_4, 1.20	18.4	Z-Scheme	108
Ti^{3+}–TiO_2/g-C_3N_4	Solar simulator	LP, CO_2 + 30% aqueous TEOA solution	CO, 38.5 CH_4, 2.36	81.7	Type II	109
Cu, P-g-C_3N_4/TiO_2	20 W LED	LP, CO_2 + 0.1 M aqueous NaOH solution	CH_3OH, 85.9	515	Z-Scheme	110
Au/C-g-C_3N_4/TiO_2	150 W Hg lamp, 400 nm filter	GP, CO_2 + H_2O	CH_4, 8.49	67.9	Type II	111
Highly deficient TiO_2 (with O vacancies)/g-C_3N_4 (with N vacancies)	300 W Xe lamp	GP, CO_2 + H_2O	CH_4, 27.4 CO, 7.5	234	Z-Scheme	112

Note. TEOA is triethanolamine; bpy is bipyridine, @ is the core@shell structure.

increasing the photocatalytic activity similarly to TiO_2/g-C_3N_4 composites.

A variety of methods for the preparation of ZnO/g-C_3N_4 composites such as hydrothermal and solvothermal synthesis, layer-by-layer deposition and other have been reported in the literature.[19] For example, Chen *et al.*[118] synthesized the ZnO/g-C_3N_4 composite photocatalyst by evaporation of a suspension consisting of a methanol solution, g-C_3N_4 and zinc acetate prepared in advance. The reduction involved CO_2 and water vapour, which were formed inside the reactor upon the reaction between $NaHCO_3$ and H_2SO_4. The W_e value found for the composite photocatalyst was 9.4 times higher than that for pristine g-C_3N_4. The use of W_e for comparison of the photocatalyst activities is especially important here, because the photocatalytic CO_2 reduction in the presence of g-C_3N_4 is dominated by the formation of CO, whereas in the case of ZnO/g-C_3N_4 composites, the reaction almost exclusively gives CH_4. The authors also studied the stability of the most active ZnO/g-C_3N_4 photocatalyst and demonstrated that the activity decreased by about 7% by the third cycle, which indicated a high stability of the synthesized photocatalyst.

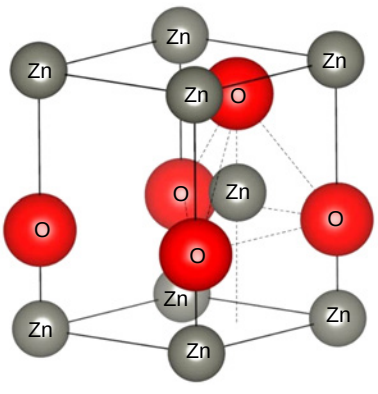

Figure 8. Crystal structure of wurtzite phase of ZnO.[115]

Guo *et al.*[119] synthesized the ZnO@g-C_3N_4 composite photocatalyst with the core@shell structure by depositing g-C_3N_4 on porous ZnO nanosheets using two-step calcination and studied the effect of reaction temperature on the photocatalyst activity towards the CO_2 reduction. A temperature rise from 150 to 200 °C resulted in a 3-fold and 2-fold increase in the rate of CH_4 and CO formation, respectively. However, as the temperature was further increased to 250 °C, the formation rate of CO_2 reduction products increased by only 33% compared to the rate at 200 °C. This effect may be caused by diffusion processes and adsorption–desorption equilibrium, which are affected by temperature. Since impossibility of initiation of photocatalytic processes by thermal energy has been proved in the literature both experimentally and theoretically, the change in the activity can be due only to the change in the above-mentioned dark stages of the reaction.[12,120–122]

Zhu *et al.*[123] deposited copper nanoparticles on the ZnO/g-C_3N_4 materials with different contents of ZnO to be used in

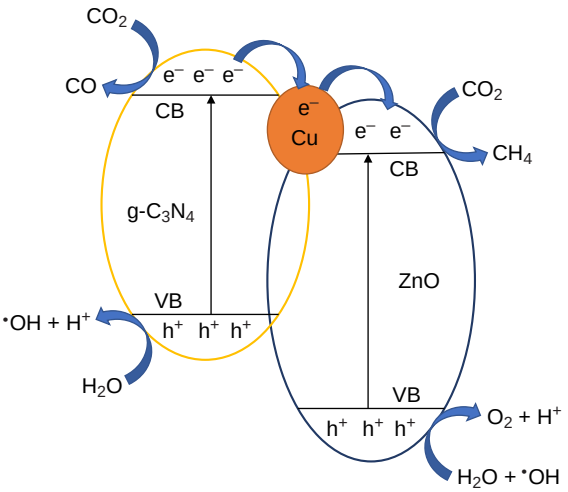

Figure 9. Possible mechanism of electron transfer in the Cu/ZnO/g-C_3N_4 heterostructures.[123]

the photocatalytic CO_2 reduction in aqueous solution under mercury lamp irradiation. The highest rates of CO, CH_4 and CH_3OH formation equal to 64, 41 and 93 μmol g^{-1} h^{-1}, respectively, were attained by using the 3% Cu/(30% ZnO/g-C_3N_4) photocatalyst.[a] These values are not only markedly higher than those for pristine g-C_3N_4, but they are also higher than those for the 30% ZnO/g-C_3N_4 composite photocatalyst. The authors proposed a possible microstructure of the 3% Cu/(30% ZnO/g-C_3N_4) photocatalyst and a mechanism of separation of the photogenerated charge carriers (Fig. 9). Presumably, the charge carrier separation mechanism implemented in the photocatalysts is similar to type II heterojunction, but occurs *via* copper nanoparticles, which act as not only electron traps, but also as sources of electrons, causing a significant increase in the photocatalytic reaction rate.

Data on some ZnO/g-C_3N_4 systems are summarized in Table 2. Currently, ZnO has been less explored for photocatalytic applications than TiO_2; hence, relatively few data on heterostructures based on ZnO composites with g-C_3N_4 have been reported in the literature. It is important that the activity of ZnO/g-C_3N_4 photocatalysts in the CO_2 reduction is at the level of TiO_2/g-C_3N_4 composite activity. Moreover, the W_e value of 1010 μmol g^{-1} h^{-1} for Cu/ZnO/g-C_3N_4 is especially notable, because three CO_2 reduction products, CO, CH_4 and CH_3OH, are formed at high rates in this case. Most types of heterojunctions present in the ZnO/g-C_3N_4 photocatalysts reported in the literature correspond to type II. However, the highest W_e value was attained for a three-component composite photocatalyst with a complex of heterojunctions.

[a] The contents of the components are given in mass percent.

2.3. Heterostructures with cerium dioxide

Cerium dioxide CeO_2 is an n-type semiconductor with a wide band gap (2.8–3.1 eV) and the fluorite structure.[128,129] An important feature of this compound is the high proneness of Ce^{4+} cations to be reduced to Ce^{3+}.[130] This change in the oxidation state results in a change in the stoichiometry and formation of oxygen vacancies, which are known to enhance the absorption of visible light and also act as photoinduced charge carrier traps or as adsorption sites (Fig. 10).[131,132]

Liang *et al.*[133] investigated hollow g-C_3N_4@CeO_2 photocatalysts for CO_2 reduction under irradiation with a xenon lamp with a 420 nm cut-off filter ($\lambda > 420$ nm). The heat treatment of the composite photocatalyst in a hydrogen atmosphere resulted in the formation of oxygen vacancies and partial Ce^{4+} reduction to Ce^{3+}. The highest rates of CH_4, CH_3OH and CO formation were attained in the presence of the g-C_3N_4@49.7%CeO_2 photocatalyst and amounted to 1.2, 1.7 and 5.6 μmol g^{-1} h^{-1}, respectively, which exceeds these values for single g-C_3N_4 and CeO_2 catalysts. The synergistic effect is caused by the formation of type II heterojunction between the

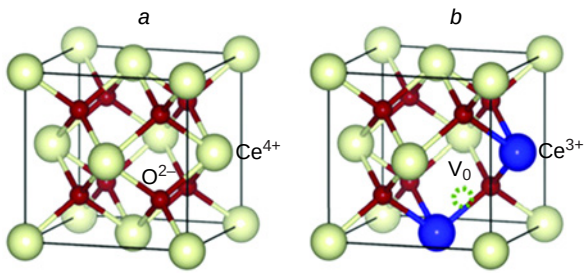

Figure 10. Crystal structure of the CeO_2 fluorite phase.[132]

Table 2. Review of some publications on CO_2 reduction in the presence of ZnO/g-C_3N_4-based photocatalysts.

Photocatalyst	Light source	Conditions	Products, formation rates, μmol g^{-1} h^{-1}	W_e, μmol g^{-1} h^{-1}	Hetero-junction	Ref.
ZnO/g-C_3N_4	300 W Xe lamp, 420 nm filter	GP, $NaHCO_3$+H_2SO_4	CO, 0.37 CH_4, 19.8	159	Type II	118
PNS-ZnO@g-C_3N_4	300 W Xe lamp, 420 nm filter	GP, CO_2+H_2O, 200 °C	CO, 16.8 CH_4, 30.5	278	Type II	119
Cu/ZnO/g-C_3N_4	400 W Hg lamp	LP, CO_2+H_2O	CO, 64.1 CH_4, 40.7 CH_3OH, 92.5	1010	Complex of junctions	123
Hollow spheres ZnO@g-C_3N_4	300 W Xe lamp	GP, $NaHCO_3$+HCl	CH_4, 16	130	S-Scheme	124
Ag/ZnO/g-C_3N_4	300 W Xe- amp, 420 nm filter	LP, CO_2+H_2O	CO, 36 CH_4, 14	180	Type II	125
Ti_3C_2/ZnO/g-C_3N_4	300 W Xe lamp	GP, CO_2+H_2O	CO, 6.41 CH_4, 0.26	14.9	Type II	126
ZnO/g-C_3N_4	300 W Xe lamp	GP, CO_2+H_2O	CO, 2.79	5.58	Type II	127

Note. PNS are porous nanosheets.

two semiconductors and by the large number of oxygen vacancies in CeO_2. The Ce^{4+} cations can trap photoinduced electrons, whereas the Ce^{3+} cations apparently provide the formation of the CO_2^- radical anion, which is an intermediate of CO_2 reduction.[134] Moreover, the hollow structure of the photocatalyst increases the light utilization efficiency due to multiple reflections.[135]

Wang *et al*.[136] synthesized a series of CeO_2/g-C_3N_4 composite photocatalysts with a built-in electric field. The electric field formation was confirmed by density functional theory (DFT) calculations. The calculation results indicate that electrons are accumulated on the g-C_3N_4 surface, while holes are concentrated on CeO_2. This gives rise to a built-in electric field directed from CeO_2 to g-C_3N_4, which promotes the transfer of photogenerated charge carriers according to the S-scheme. The highest product formation rates attained on the 1.75% CeO_2/g-C_3N_4 photocatalyst were 0.56 and 15 μmol g^{-1} h^{-1} for CO and CH_4, respectively, which is almost 20 times higher than those attained with single g-C_3N_4 or CeO_2.

Li *et al*.[137] reported a multistep hydrothermal synthesis of the CeO_2/g-C_3N_4 composite photocatalyst; then partially reduced graphene oxide (rGO) was deposited on the composite surface. Partially reduced graphene oxide is a graphene-like material with specific structural defects and oxidized groups on the surface.[138] The combination of these characteristics gives rise to a two-dimensional material with a large specific surface area, high electron mobility and chemical stability, which makes it a promising component for the synthesis of composite photocatalysts.[139] The photocatalytic CO_2 reduction was carried out in a suspension consisting of an alkaline solution of TEOA and a photocatalyst under xenon lamp irradiation. The CO and CH_4 formation rates were 63 and 33 μmol g^{-1} h^{-1} for rGO/CeO_2/g-C_3N_4 *vs* 15 and 5.2 μmol g^{-1} h^{-1} for g-C_3N_4. The results of DFT calculations suggest the formation of a built-in electric field in the composite photocatalyst caused by changes in the Fermi levels, similarly to what was described by Li *et al*.[137] In the resulting multicomponent heterostructure, the formation of S-scheme heterojunction for electrons was suggested.

Data on the CeO_2/g-C_3N_4 systems are summarized in Table 3. The use of CeO_2 in photocatalytic studies is primarily due to the variable stoichiometry. The highest W_e values for CeO_2-based composite photocatalysts were obtained for heterostructures in which the charge carrier separation mechanism corresponds to the S-scheme and which are used for liquid-phase CO_2 reduction. As can be seen from Table 3, the formation of S-scheme heterojunction provides the highest activity of CeO_2/g-C_3N_4-based photocatalysts. However, the activity of photocatalysts of this type is usually lower than that of TiO_2/g-C_3N_4 or ZnO/g-C_3N_4. Apparently, CeO_2 may be a promising material for the synthesis of photocatalysts for CO_2 reduction; however, additional studies along this line are needed.

2.4. Heterostructures with iron oxide α-Fe_2O_3

The iron oxide α-Fe_2O_3 (hematite) is a readily available, thermodynamically stable and environmentally benign narrow-band-gap n-type semiconductor.[146–149] However, the narrow band gap (2.2 eV) not only enhances the visible light absorption, but also markedly decreases the lifetime of photogenerated electron–hole pairs.[150] Moreover, the energy level of the bottom of the conduction band hampers the use of this material in reduction reactions due to the low potential of photogenerated electrons.[19,151] Thus, α-Fe_2O_3 can be used in the photocatalytic CO_2 reduction only upon the formation of heterostructures with other semiconductors. In this respect, g-C_3N_4 can act as a semiconductor with an appropriate level of the conduction

Table 3. Review of some studies on CO_2 reduction in the presence of CeO_2/g-C_3N_4-based photocatalysts.

Photocatalyst	Light source	Conditions	Products, formation rates, μmol g^{-1} h^{-1}	W_e, μmol g^{-1} h^{-1}	Hetero-junction	Ref.
Hollow g-C_3N_4@CeO_2	300 W Xe lamp, 420 m filter	GP, CO_2 + H_2O	CO, 5.60 CH_4, 1.2 CH_3OH, 1.7	31	Type II	133
CeO_2/g-C_3N_4 with an internal electric field	300 W Xe lamp, 400 nm filter	LP, CO_2 + 10% aqueous solution of TEOA	CO, 0.56 CH_4, 14.6	118	S-Scheme	136
rGO/CeO_2/g-C_3N_4	300 W Xe lamp	LP, CO_2 + 1 M aqueous NaOH + 1 M TEOA solution	CO, 63.2 CH_4, 32.7	388	S-Scheme	137
Pt/CeO_2/g-C_3N_4	300 W UV lamp	LP, CO_2 + 0.1 M aqueous NaOH + 1% TEOA solution	CO, 4.69 CH_4, 3.03	33.6	Type II	140
Ag/m-CeO_2/g-C_3N_4	8 W UV lamp	LP, CO_2 + 0.1 M aqueous NaOH + TEOA	CO, 13.9 CH_4, 7.39	87	Complex of junctions	141
(Phosphate-modified octahedral CeO_2 {111})/g-C_3N_4	300 W Xe lamp	LP, CO_2 + H_2O	CO, 4.18	8.37	Z-Scheme	142
CeO_2/g-C_3N_4	300 W Xe lamp	GP, CO_2 + H_2O	CO, 8.99 CH_4, 0.6	22.8	Z-Scheme	143
(g-C_3N_4 quantum dots)/m-CeO_2	8 W UV lamp	LP, 0.1M aqueous NaOH + 1% TEOA solution	CO, 2.25 CH_4, 1.58	17.1	Type II	144
CeO_2/g-C_3N_4	300 W Xe lamp, 400 nm filter	GP, CO_2 + H_2O	CO, 3.88 CH_4, 0.149	8.95	Type II	145

Note. m is mesoporous.

band minimum and with wider band gap compared to that of α-Fe_2O_3.

Guo *et al.*[152] used the hydrothermal method to prepare the α-Fe_2O_3/g-C_3N_4 composite for the photocatalytic CO_2 reduction to CH_3OH in water under xenon lamp irradiation with a 420 nm cut-off filter. The highest CH_3OH formation rate is 5.6 μmol g^{-1} h^{-1}, which is almost three times higher than that for pristine g-C_3N_4 (1.9 μmol g^{-1} h^{-1}). This increase is attributable to the formation of direct Z-scheme, which prevents recombination of photogenerated charge carriers and promotes the generation of electrons with a high reduction potential.

Duan and Mei[153] synthesized the α-Fe_2O_3/g-C_3N_4 photocatalyst by hydrothermal method from a colloidal solution containing both components (Fig. 11). The CO_2 reduction reaction was conducted in an aqueous solution of DMF and TEOA under irradiation with a 60 W white light emitting diode (LED). The major reaction product was CH_3OH formed at a high rate of 74 μmol g^{-1} h^{-1}. The solvent effect on the reaction rate was investigated by replacing DMF with acetonitrile, but the photocatalyst activity significantly decreased, indicating that the use of DMF in the photocatalytic CO_2 reduction may be promising for α-Fe_2O_3/g-C_3N_4 photocatalysts (but not necessarily for other ones[154]). It is worth noting that under the light irradiation, TEOA can be converted in the reaction medium to give carbon-containing products, which can affect the photocatalytic reaction rate.[155–158] This effect was ruled out by conducting an experiment with $^{13}CO_2$; this confirmed that CO_2 was the only source of CH_3OH.

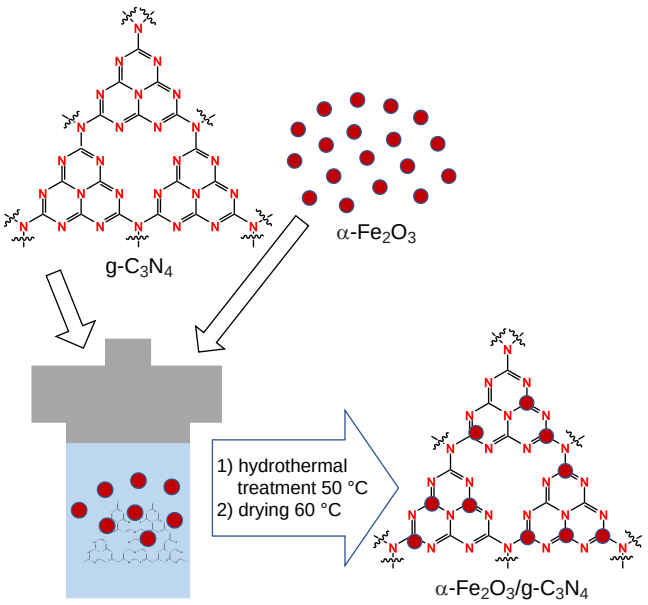

Figure 11. Schematic image of the synthesis of the α-Fe_2O_3/g-C_3N_4 photocatalyst.[153]

Padervand *et al.*[159] synthesized a complex composite photocatalyst, $K_4Nb_6O_{17}$/Fe_3N/α-Fe_2O_3/C_3N_4, by one-step thermal pyrolysis of the precursor. The photocatalyst combines the properties of three semiconductors with different positions of bands and magnetic properties of Fe_3N, which produces a highly efficient system for photocatalytic reactions. The highest product formation rates in the gas-phase CO_2 reduction under visible light irradiation were 7.0 and 1.3 μmol g^{-1} h^{-1} for CO and CH_4, respectively. The authors also proposed an electron transfer mechanism: since $K_4Nb_6O_{17}$ has a wider band gap with a very low top of valence band , type I heterojunction with α-Fe_2O_3 can be formed simultaneously with S-scheme heterojunction between α-Fe_2O_3 and g-C_3N_4. Moreover, Fe_3N acts as an electron trap, similarly to metals. These features explain the high CO_2 conversion upon photocatalyst irradiation with visible light.

Data on α-Fe_2O_3/g-C_3N_4 systems reported recently are summarized in Table 4. The highest W_e value of 440 μmol g^{-1} h^{-1} was found for the reaction in an aqueous solution of DMF + TEOA, whereas standard conditions of CO_2 reduction in aqueous solutions or in the presence of water vapour resulted in a lower rate, even when complex heterostructures were used as photocatalysts. Thus, the formation of composite photocatalysts consisting of g-C_3N_4 and narrow-band-gap semiconductors such as α-Fe_2O_3 is not a promising trend. In this case, high rates of product formation are not attained, probably because of the low lifetime of photogenerated charge carriers caused by the narrow band gaps of both components.

3. Heterostructures with metal sulfides

3.1. Heterostructures with cadmium sulfide

Cadmium sulfide CdS is a semiconductor material widely used for photocatalytic CO_2 reduction and many other photocatalytic reactions, because it has a narrow band gap (~2.4 eV) and appropriate arrangement of the valence and conduction bands.[162–165] Meanwhile, the photocatalytic application of CdS is limited not only by recombination of electron–hole pairs, but also by photocorrosion caused by the oxidation of sulfide ions by photogenerated holes.[166–169] An effective method to overcome these drawbacks is to fabricate composite photocatalysts based on CdS and other semiconductors.

Table 4. Review of some studies on CO_2 reduction in the presence of α-Fe_2O_3/g-C_3N_4-based photocatalysts.

Photocatalyst	Light source	Conditions	Products, formation rates, μmol g^{-1} h^{-1}	W_e, μmol g^{-1} h^{-1}	Hetero-junction	Ref.
α-Fe_2O_3/g-C_3N_4	300 W Xe lamp, 420 nm filter	LP, CO_2 + H_2O	CH_3OH, 5.63	33.8	Z-Scheme	152
α-Fe_2O_3/g-C_3N_4	60 W white LED	LP, CO_2 + aqueous DMF + TEOA solution	CH_3OH, 73.7	442	Z-Scheme	153
$K_4Nb_6O_{17}$/ Fe_3N/α-Fe_2O_3/g-C_3N_4	300 W Xe lamp, 420 nm filter, 0.22 W cm^{-2}	GP, CO_2 + H_2O	CO, 7.01 CH_4, 1.3	24	S-Scheme, Type I, Type II	159
Fe_3N/α-Fe_2O_3/g-C_3N_4	300 W Xe lamp, 420 nm filter, 0.22 W cm^{-2}	GP, CO_2 + H_2O	CO, 8.03 CH_4, 1.6	29	Z-Scheme	160
α-Fe_2O_3/g-C_3N_4	300 W Xe lamp	GP, CO_2 + H_2O	CO, 17.8	35.6	Z-Scheme	161

Vu *et al.*[170] synthesized the CdS/g-C_3N_4 composite and studied it in the photocatalytic CO_2 reduction under irradiation with a solar simulator (100 mW cm^{-2}); the photocatalyst was suspended in a solution containing acetonitrile, TEOA, water and $[Co(bpy)_3]Cl_2$. An aqueous solution of acetonitrile was used as a solvent, TEOA served as an electron donor and the organometallic complex acted as a co-catalyst. It is noteworthy that no CO_2 reduction products were detected in the absence of TEOA and the Co complex. Carbon monoxide was formed as the major product of CO_2 reduction, CH_4 was detected in a small amount, and H_2 was formed as a by-product. The rate of CO evolution was 240 μmol g^{-1} h^{-1}, which was almost four times higher than that with pristine g-C_3N_4. The selectivity to CO was 73%. The photocorrosion of CdS was inhibited *via* migration of photogenerated holes to g-C_3N_4: study of the photocatalyst stability indicated no loss of activity after four reaction cycles. The synergistic effect of CdS/g-C_3N_4 heterostructure is attributable to implementation of the direct Z-scheme with a bridging C–S–Cd bond at the interface, which results in increasing rate of transfer and separation of photogenerated charge carriers (Fig. 12).

Guo *et al.*[171] synthesized a photocatalyst based on g-C_3N_4 and $Zn_{0.2}Cd_{0.8}S$ nanoparticles using a combination of ultrasonic treatment and hydrothermal method (Fig. 13). The $Zn_xCd_{1-x}S$ solid solutions are known as photocatalysts that are activated under visible light and have a tunable band structure, which can be controlled by varying the Zn : Cd ratio, as in other solid solutions.[172–175] The photocatalytic activity in the CO_2 reduction was measured in an aqueous suspension of the photocatalyst at 80 °C under irradiation with a xenon lamp with a 420 nm cut-off filter. Methanol was the only detected product, which formed at a rate of 12 μmol g^{-1} h^{-1}; this was higher than the methanol formation rate in the reaction performed using single components of the photocatalyst. Stability testing showed a decrease in the activity by only 7% after 28 h of the reaction, which indicated successful inhibition of photocorrosion. The authors suggested that separation of the photogenerated charge carriers in this photocatalyst corresponds to type II heterojunction, which promotes increase in both stability and activity.

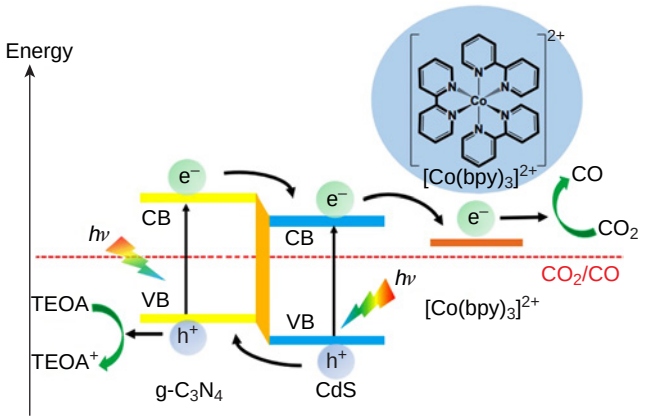

Figure 12. Mechanism of the photoinduced electron transfer in the CdS/g-C_3N_4 photocatalysts in a solution with $[Co(bpy)_3]Cl_2$.[170] Published with permission from the American Chemical Society.

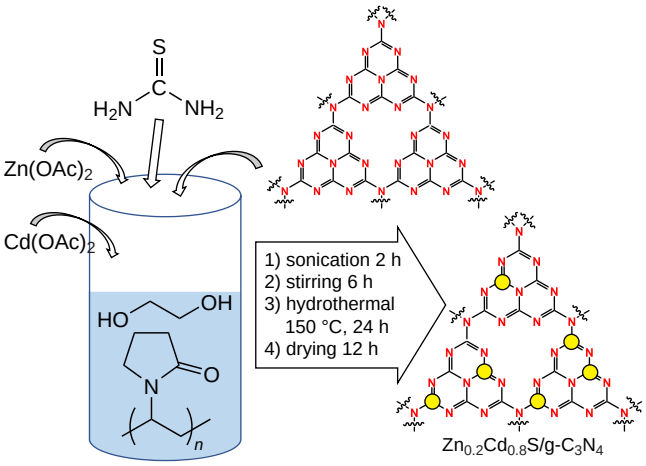

Figure 13. Schematic image of the synthesis of the $Zn_{0.2}Cd_{0.8}S$/g-C_3N_4 photocatalyst.[171]

Data on some CdS/g-C_3N_4-based systems are summarized in Table 5. Since CdS is also a narrow-band-gap semiconductor, its combination with g-C_3N_4 usually does not provide high rates of CO_2 reduction. To attain high activity, additional modification or more complex reaction system is required. In particular, the two highest W_e values were found for systems using m-CdS/g-C_3N_4 photocatalyst dispersed in a solution, whereas W_e observed for the gas-phase CO_2 reduction in the presence of $(Au/Zn_xCd_{1-x}S)$@g-C_3N_4 was only 7.9 μmol g^{-1} h^{-1}.

3.2. Heterostructures with tin sulfide

Tin disulfide SnS_2 is a non-toxic semiconductor with a narrow band gap (~2.2 eV); therefore, it may be of interest for

Table 5. Review of some studies on CO_2 reduction in the presence of CdS/g-C_3N_4-based photocatalysts.

Photocatalyst	Light source	Conditions	Products, formation rates, μmol g^{-1} h^{-1}	W_e, μmol g^{-1} h^{-1}	Hetero-junction	Ref.
CdS/g-C_3N_4	Solar simulator, 100 mW cm^{-2}	LP, CO_2 + MeCN+H_2O + TEOA + $[Co(bpy)_3]Cl_2$	CO, 235	469	TypeII	170
$Zn_{0.2}Cd_{0.8}S$/g-C_3N_4	300 W Xe lamp, 420 nm filter	LP, CO_2 + H_2O, 80 °C	CH_3OH, 11.5	69.0	Type II	171
m-CdS/g-C_3N_4	300 W Xe lamp, 420 nm filter	LP, aqueous solution of Na_2CO_3 + HCl	CH_3OH, 193	1160	Z-Scheme	176
CdS/Au/g-C_3N_4/halloysite nanotubes	UV/Vis light	LP, CO_2 + 5% aqueous solution of TEOA	CO, 13.9 CH_4, 2.2	45	Type II	177
$(Au/Zn_xCd_{1-x}S)$@g-C_3N_4	300 W Xe lamp, 420 nm filter	GP, $NaHCO_3$ + H_2SO_4	CH_3OH, 1.31	7.86	Z-Scheme	178

photocatalytic studies as a combination with wider-band-gap semiconductors.[179–184]

Wang *et al.*[185] synthesized SnS_2/g-C_3N_4 composite photocatalysts with type II heterojunction by using self-assembly based on the electrostatic interactions between the components in an ethanol solution. The prepared photocatalysts with different SnS_2 contents were tested in the photocatalytic CO_2 reduction under xenon lamp irradiation. The highest rate of formation of the major product (CO) was 0.64 μmol g^{-1} h^{-1} in the presence of 60%SnS_2/g-C_3N_4, which is much higher than the rates attained using single g-C_3N_4 or SnS_2. The stability testing carried out for the most active sample showed that the activity remained almost unchanged after four cycles of the photocatalytic reaction. Since the results of X-ray diffraction and X-ray photoelectron spectroscopy did not show any significant changes either, it can be assumed that the synthesized photocatalyst has a high photocatalytic stability. Study of the charge carrier transfer mechanism provided the conclusion that type II heterojunction is formed between g-C_3N_4 and SnS_2. This increases the charge carrier separation rate, but, simultaneously, it also leads to a decrease in the redox potentials of photogenerated electrons and holes.

Yin *et al.*[186] obtained the SnS_2/g-C_3N_4 composite photocatalyst by a two-step method comprising sonication and hydrothermal synthesis followed by photodeposition of Au nanoparticles. The resulting photocatalyst was studied in CO_2 reduction in an aqueous solution of TEOA under irradiation with a xenon lamp. The major reaction products were CO and CH_4, with their formation rates being 94 and 75 μmol g^{-1} h^{-1}, respectively, while g-C_3N_4 and SnS_2 taken separately had lower activity. The synergistic effect is due to two factors. First, both the hydrophilicity and CO_2 adsorption increase in the series g-C_3N_4 < SnS_2 < SnS_2/g-C_3N_4 < SnS_2/Au/g-C_3N_4, which leads to increasing adsorption of the reactants on the photocatalyst surface. Second, it is assumed that gold nanoparticles act as electron mediators for the Z-scheme implemented in the composite photocatalyst, which facilitates the electron transfer and increases the rate of charge carrier separation.

SnS_2 is not the only tin sulfide that is used as a photocatalyst. For example, Huo *et al.*[187] reported hydrothermal synthesis of a composite photocatalyst consisting of porous g-C_3N_4 and Sn_2S_3 modified with diethylenetriamine (DETA) (Fig. 14). The CO_2 reduction experiment was carried out in the gas phase in which CO_2 and water were formed upon the reaction of $NaHCO_3$ with HCl. A xenon lamp with a >420 nm cut-off filter was used as the light source. The major reaction products were CH_4 and CH_3OH, with the rates of their formation being 4.9 and 1.5 μmol g^{-1} h^{-1}, respectively; this is higher than the activities of the initial g-C_3N_4 and Sn_2S_3-DETA. The replacement of H_2SO_4 by HCl did not result in any noticeable change in the reaction rate, which implies that the acid is not involved in the photocatalytic reaction. It is assumed that the synergistic effect is due to implementation of direct Z-scheme in the synthesized composite photocatalyst with a built-in electric field.

The data on the systems based on tin sulfides and g-C_3N_4 are summarized in Table 6. Despite the fact that the tin sulfide band

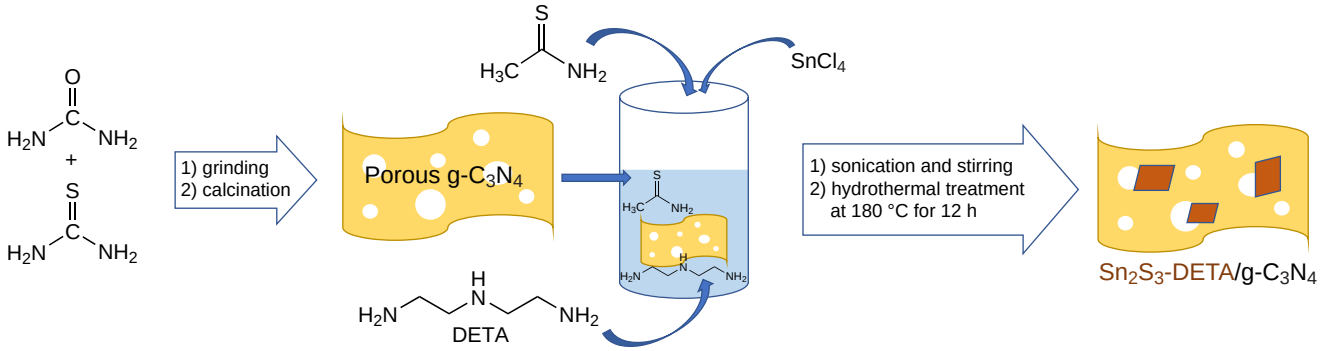

Figure 14. Schematic image of the synthesis of the Sn_2S_3-DETA/g-C_3N_4 photocatalyst.[187]

Table 6. Review of some studies on CO_2 reduction in the presence of photocatalysts based on tin sulfides and g-C_3N_4.

Photocatalyst	Light source	Conditions	Products, formation rates, μmol g^{-1} h^{-1}	W_e, μmol g^{-1} h^{-1}	Hetero-junction	Ref.
SnS_2/g-C_3N_4	300 W Xe lamp	LP, CO_2 + H_2O	CO, 0.64	1.27	Type II	185
SnS_2/Au/g-C_3N_4	300 W Xe lamp	LP, CO_2 + aqueous solution of TEOA	CO, 93.8 CH_4, 75.0	788	Z-Scheme	186
Sn_2S_3-DETA/g-C_3N_4	300 W Xe lamp, 420 nm filter	GP, $NaHCO_3$ + HCl	CH_4, 4.93 CH_3OH, 1.49	48.4	Z-Scheme	187
SnS_2/g-C_3N_4/C hollow spheres	300 W Xe lamp	GP, CO_2 + H_2O	CO, 40.9	81.7	Z-Scheme	188
SnS_2-SnO_2/S-g-C_3N_4	300 W Xe lamp, AM1.5G filter, 100 mW cm^{-2}	GP, CO_2 + H_2O	CO, 23.2 CH_4, 21.2	216	Type II	189
SnS/g-C_3N_4	100 W Xe lamp, AM1.5G filter	GP, CO_2 + H_2O	CH_4, 122	978	Z-Scheme	190
Cu_2SnS_3/g-C_3N_4	100 W Xe lamp, AM1.5G filter	GP, CO_2 + H_2O	CO, 18.2	36.4	Z-Scheme	191

Note. AM1.5G filter is a filter to obtain the spectrum corresponding to the AM1.5G standard.

gap is narrower than that of g-C_3N_4, tin sulfides (II, III, IV) are also used to form heterostructures. Apparently, SnS is potentially the most appropriate photocatalyst in this series for the photocatalytic CO_2 reduction, because the highest W_e value of 980 μmol g^{-1} h^{-1} was observed for SnS/g-C_3N_4 system in the gas-phase reduction of CO_2 under irradiation with a solar simulator. For comparison, the SnS_2/g-C_3N_4 system modified by gold nanoparticles, which was tested in the liquid-phase reduction of CO_2 under irradiation with full-spectrum xenon lamp, provided W_e of 790 μmol g^{-1} h^{-1}. Note that tin sulfides are not widely used for the synthesis of heterostructures with g-C_3N_4, and there are few publications describing the use of tin sulfides as photocatalytic materials for CO_2 reduction, although SnS-based photocatalysts can potentially exhibit a fairly high activity in other reactions, for example, decomposition of dyes.[192]

4. Heterostructures with 2D materials

4.1. Heterostructures with MXenes

MXenes are a new class of 2D metal carbides, nitrides or carbonitrides discovered in 2011.[193] As a rule, MXenes are obtained from MAX phases by removing layers of A element (usually Al) with a potent etching reagent containing F^- anions (Fig. 15).[193–198] Different methods of synthesis result in the formation of different surface functional groups (*e.g.*, –O, –F, –OH and –Cl). The general formula of MXenes can be written as $M_{n+1}X_nT_x$, where M is transition metal, X is C or N, and T is a functional group. MXenes have a number of remarkable properties such as high electrical conductivity, hydrophilicity and ordered layered structure, also, the composition of functional groups on their surface can be controlled.[197,198] MXenes have already proved to possess a high potential for many applications including photocatalysis and are considered as promising materials for photocatalytic CO_2 reduction, especially in combination with other semiconductors forming heterostructures. The electronic structure of MXenes is characterized, most often, by the absence of band gap and high electron work function; therefore, they can be used as co-catalysts to form Schottky junction at the semiconductor–MXene interface, similarly to heterostructures based on transition metals and semiconductors.[199]

Li *et al.*[200] developed mesoporous $Ti_3C_2T_x$/g-C_3N_4 photocatalysts for CO_2 reduction under irradiation with a xenon lamp (Fig. 16). The MXene phase was prepared by a widely used method involving etching of Ti_3AlC_2 with hydrofluoric acid to remove Al layers. The reduction of CO_2 in the presence of $Ti_3C_2T_x$/g-C_3N_4 gave CO and CH_4 as the major products, with the formation rates being 4.0 μmol g^{-1} h^{-1} for CO and 2.2 μmol g^{-1} h^{-1} for CH_4; these values attained with mesoporous g-C_3N_4 were 3.1 and 0.88 μmol g^{-1} h^{-1}, respectively. This effect is attributable to higher specific surface area, larger number of defects, higher electron transfer rate and, consequently, lower recombination rate of photogenerated charge carriers.

M.Tahir and B.Tahir[201] synthesized a composite material consisting of g-C_3N_4 and layered bentonite clay (Bt), on which Ti_3C_2 particles were then deposited using the ultrasonic self-

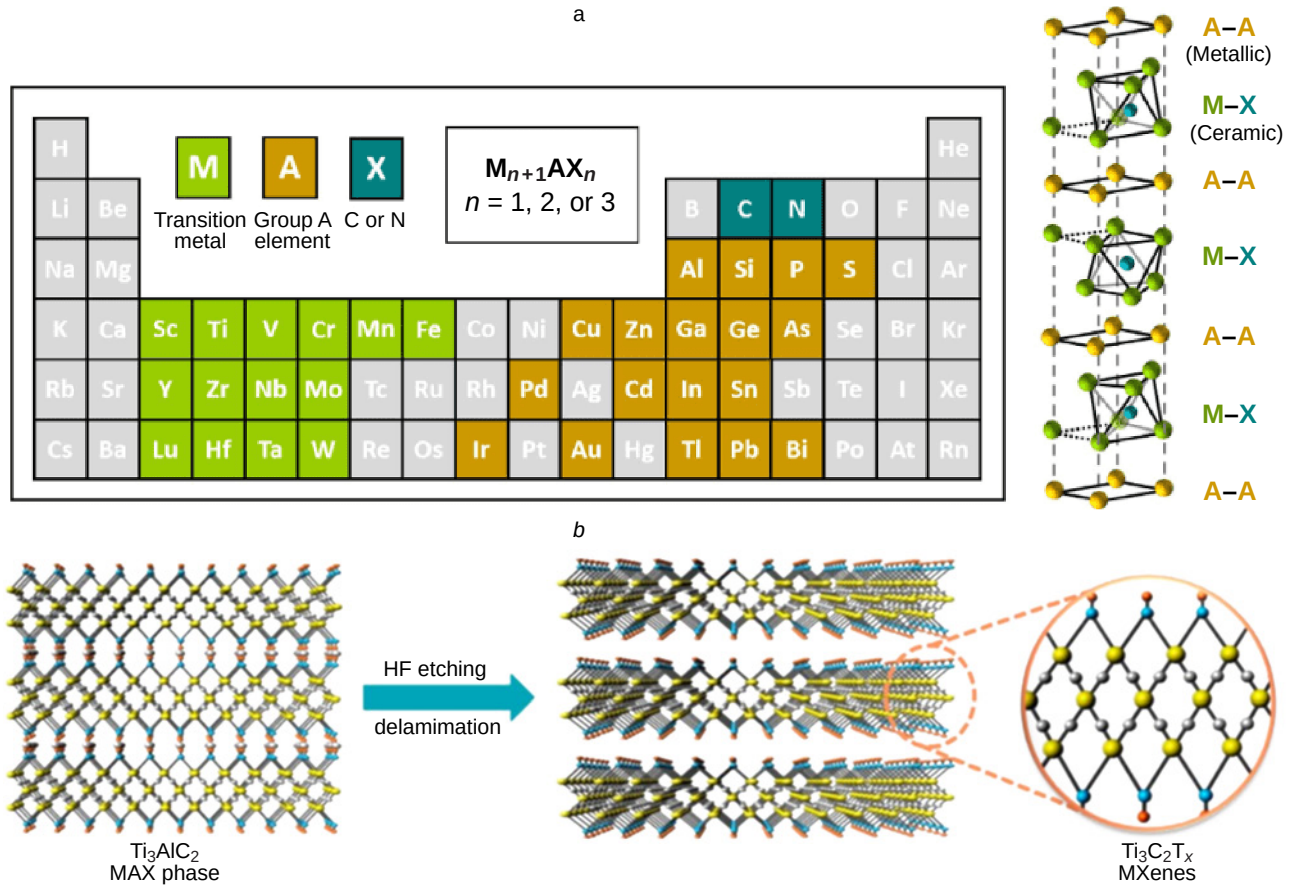

Figure 15. Periodic Table of Elements with highlighted elements present in other MAX phases (*a*)[198] and basic diagram of MXene synthesis (*b*).[198]

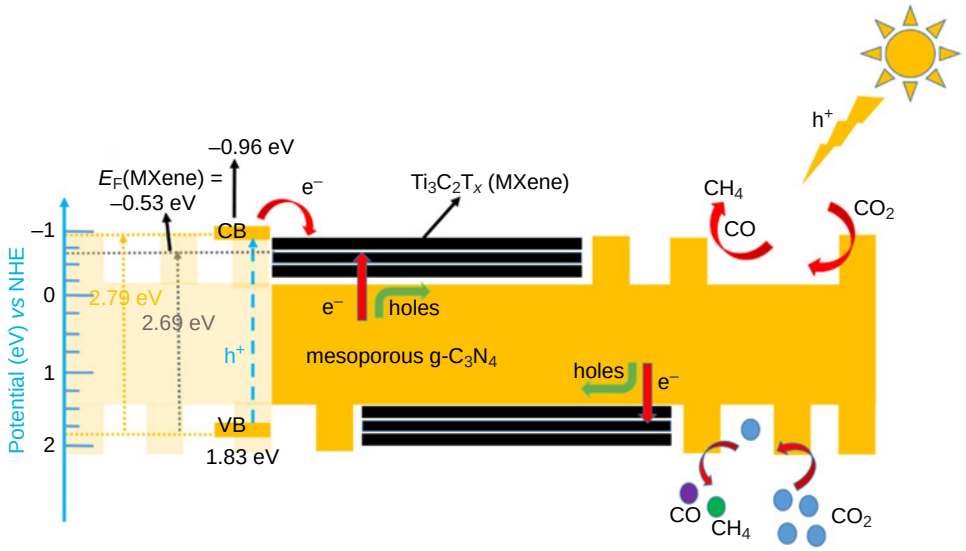

Figure 16. Schematic image of processes that take place in the $Ti_3C_2T_x$/g-C_3N_4 photocatalyst.[200]

assembly technique. Bentonite mainly consists of smectite minerals, particularly montmorillonite (usually Ca montmorillonite and Na montmorillonite),[202] has a columnar multilayer structure and can significantly enhance CO_2 adsorption and charge carrier separation rate owing to bentinite surface properties and the presence of metal cations, which increase the photocatalytic activity (Fig. 17).[202,203] Indeed, the photocatalytic experiments on CO_2 reduction demonstrate that the Ti_3C_2/g-C_3N_4/Bt ternary composite provides a much higher rates of formation of the major products (CO and CH_4), especially CH_4. It is presumed that the increase in the selectivity to CH_4 is caused by the efficient heterotransfer of charge carriers between the phases, which promotes the eight-electron reduction of CO_2 to CH_4. The effect of a sacrificial agent is also investigated, and it is found that the addition of acetic acid increases the rate of CH_4 formation by a factor of 4.2. CH_3COOH acts as an electron donor, decreases the charge carrier recombination rate and serves as a source of H_2, which is a more thermodynamically favourable reagent for CO_2 reduction than water.[203–207]

Studies dealing with composite photocatalysts for CO_2 reduction based on other MXenes, apart from Ti_3C_2, have also been reported. For example, Madi *et al.*[208] synthesized the V_2C/g-C_3N_4 photocatalyst by physical mixing of the components and sonication. The activity of the resulting photocatalyst in the gas-phase reduction of CO_2 under irradiation with a 35 W xenon lamp was considerably higher than the activity of g-C_3N_4 and somewhat higher than the activity of V_2AlC/g-C_3N_4. The authors attributed this synergistic effect to high electronic conductivity, which is one of the main benefits of V_2C and to the formation of Schottky junction between g-C_3N_4 and V_2C, which promotes the separation of photogenerated charge carriers.[209–213] A drawback of the composite is low stability: the photocatalyst activity decreases with every irradiation cycle, with the decrease reaching 40% by the end of the third cycle.

Data on the MXene/g-C_3N_4-based systems are summarized in Table 7. Analysis shows that, unfortunately, modification of g-C_3N_4 with Ti_3C_2 does not lead to a significant increase in the activity. It is noteworthy that data on the gas-phase CO_2 reduction giving CO and CH_4 as the major products are mainly presented in the literature. An outstanding W_e value of 8400 μmol g^{-1} h^{-1} was attained for the system containing bentonite clay under irradiation with a xenon lamp and with addition of acetic acid to the reaction system. A relatively simple V_2C/g-C_3N_4 heterostructure had W_e of 490 μmol g^{-1} h^{-1}, which far exceeded the activity of most Ti_3C_2/g-C_3N_4 systems. It can

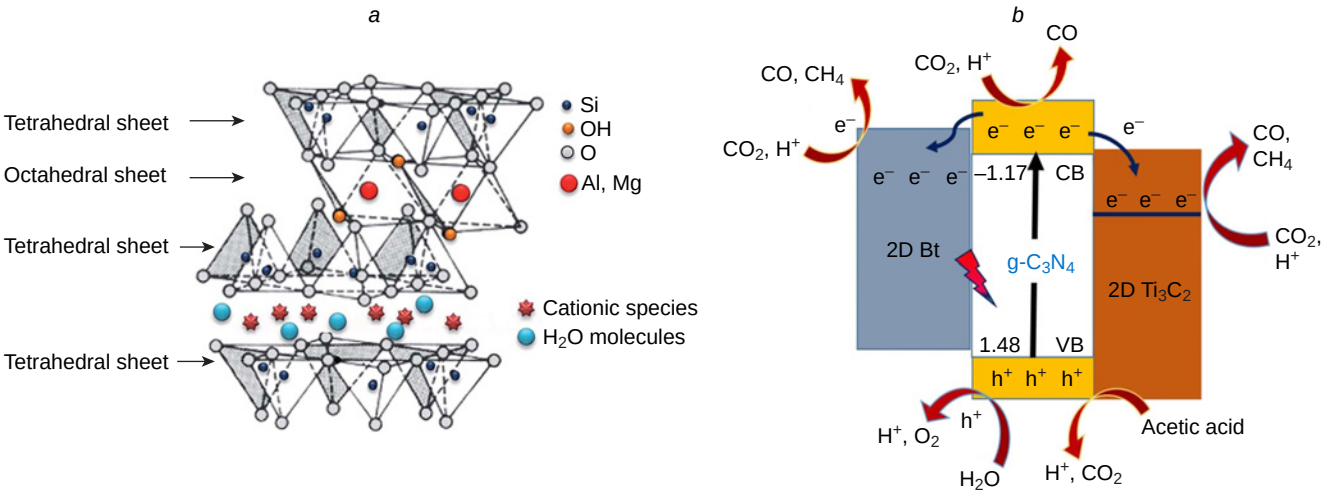

Figure 17. (*a*) Structure of bentonite; (*b*) schematic image of processes taking place in the Ti_3C_2/g-C_3N_4/Bt photocatalyst.[202,203]

Table 7. Review of some studies on CO_2 reduction in the presence of photocatalysts based on MXene/g-C_3N_4.

Photocatalyst	Light source	Conditions	Products, formation rates, μmol g^{-1} h^{-1}	W_e, μmol g^{-1} h^{-1}	Hetero-junction	Ref.
$Ti_3C_2T_x$/g-C_3N_4	300 W Xe lamp, 200 mW cm^{-2}	GP, $NaHCO_3$ + H_2SO_4	CO, 0.73 CH_4, 1.4	13	Schottky	93
Ti_3C_2/g-C_3N_4/TiO_2	350 W Xe lamp	GP, $NaHCO_3$ + H_2SO_4	CO, 4.39 CH_4, 1.20	18.4	S-Scheme	108
Ti_3C_2/ZnO/g-C_3N_4/	350 W Xe lamp	GP, CO_2 (0.02 MPa) + H_2O	CO, 6.41 CH_4, 0.26	14.9	Type II+ Schottky	126
$Ti_3C_2T_x$/m-g-C_3N_4	350 W Xe lamp	GP, CO_2 + H_2O	CO, 3.98 CH_4, 2.12	24.9	Schottky	200
Ti_3C_2/g-C_3N_4/Bt	350 W Xe lamp	GP, H_2O + CO_2 + CH_3COOH	CO, 365 CH_4, 955	8370	Schottky	201
V_2C/g-C_3N_4	35 W Xe lamp, 20 mW cm^{-2}	GP, CO_2 + H_2O	CO, 37.8 CH_4, 51.3	486	Schottky	208
Ti_3C_2/g-C_3N_4	300 W Xe lamp, 420 nm filter	GP, $NaHCO_3$ + H_2SO_4	CO, 5.19 CH_4, 0.044	10.7	Schottky	214
$Ti_3C_2(OH)_x$/g-C_3N_4	300 W Xe lamp, 420 nm filter	GP, CO_2 + H_2O	CO, 11.2 CH_4, 0.203	24.0	Schottky	215
g-C_3N_4/$Ti_3C_2T_x$/TiO_2	300 W Xe lamp	GP, CO_2 + H_2O	CO, 8.65 CH_4, 1.23	27.1	S-Scheme	216
Ti_3C_2/g-C_3N_4	300 W Xe lamp, 420 nm filter	LP, CO_2 + H_2O, 60 °C	CH_4, 0.99	7.92	Schottky	217
Ti_3C_2/B-g-C_3N_4	300 W Xe lamp, 420 nm filter, 175 mW cm^{-2}	GP, CO_2 + H_2O	CO, 14.4 CH_4, 0.8	35	Schottky	218

be concluded that MXenes have a great potential as co-catalysts for photocatalytic CO_2 reduction and that intensive research along this line is needed.

4.2. Heterostructures with partially reduced graphene oxide

As mentioned above, partially reduced graphene oxide (rGO) is a promising material for photocatalysis due to its excellent conductivity and mechanical and optical properties combined with ready availability and the ease of synthesis from graphene oxide (GO).[138] Moreover, a change in the reduction conditions makes it possible to obtain rGO samples that markedly differ in properties.[219] A traditional method for rGO production is the modified Hummers method, in which graphite is chemically oxidized and then exfoliated to produce graphene oxide.[220] In this stage, oxygenated functional groups appear in the graphene layers (Fig. 18).[221] During the subsequent reduction, some of these groups are removed, and the degree of reduction varies depending on the conditions.[222] It is noteworthy that the production of graphene oxide is accompanied by not only the formation of numerous oxygenated groups on the surface, but also by disruption of the conjugated structure of graphene, which provides for high mobility of charge carriers. The reduction of graphene oxide leads to the partial removal of oxygenated groups and restores the conjugated structure.[223]

Li *et al.*[224] performed a two-step process consisting of calcination and hydrothermal treatment and thus synthesized a composite photocatalyst by combining g-C_3N_4 and rGO with pre-treated multi-walled carbon nanotubes (P-MWNT).[224] The photocatalytic CO_2 reduction was carried out under xenon lamp irradiation with a 420 nm cut-off filter in a TEOA and acetonitrile solution. The highest rates of CO and CH_4 formation were 180 and 120 μmol g^{-1} h^{-1}, respectively. The authors proposed a possible structure of the photocatalyst in which carbon nanotubes act as a mediator between g-C_3N_4 and rGO and increase the rate of electron transfer. Presumably, photogenerated electrons migrate from g-C_3N_4 to rGO (either directly or *via* P-MWNT) as a result of generation of a built-in electric field, which considerably increases the efficiency of separation of photogenerated charge carriers.[225,226]

Bafaqeer *et al.*[227] used the three-component rGO-bridged ZnV_2O_6/g-C_3N_4 photocatalyst for the photocatalytic conversion of CO_2 to CH_3OH in water. For experiments, the authors designed an externally reflected photoreactor to increase the efficiency of photon energy utilization. As a result, the highest

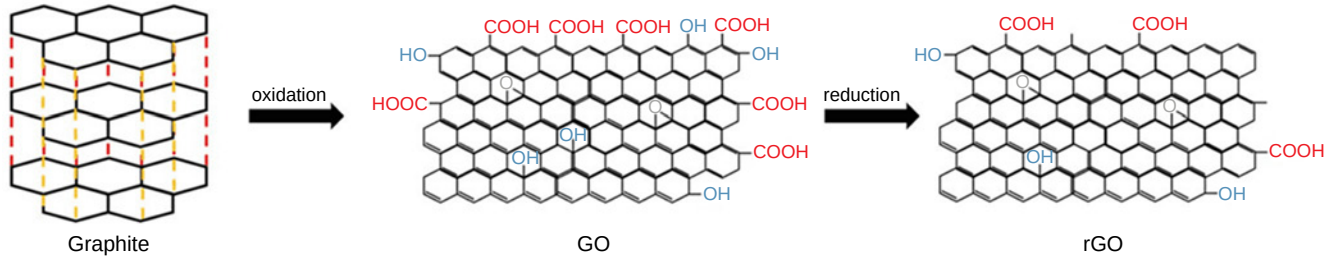

Figure 18. Schematic image of graphite oxidation and subsequent reduction to rGO.[221]

Table 8. Review of some studies on CO_2 reduction in the presence of rGO/g-C_3N_4-based photocatalysts.

Photocatalyst	Light source	Conditions	Products, formation rates, μmol g^{-1} h^{-1}	W_e, μmol g^{-1} h^{-1}	Hetero-junction	Ref.
rGO/CeO_2/g-C_3N_4	300 W Xe lamp	LP, aqueous solution of NaOH + TEOA	CO, 63.2 CH_4, 32.7	388	S-Scheme	137
g-C_3N_4/P-MWNT/rGO	300 W Xe lamp, 420 nm filter	LP, aqueous solution of TEOA + C_2H_3N	CO, 175 CH_4, 120	1310	Schottky	224
ZnV_2O_6/rGO/g-C_3N_4	35 W Xe lamp, 20 mW cm^{-2}	LP, water; externally reflected reactor	CH_3OH, 625	3750	S-Scheme	227
NiAl-LDH/rGO/g-C_3N_4	300 W Xe lamp, 1000 mW cm^{-2}	LP, aqueous solution of CH_3CN + TEOA	CO, 2.6 CH_4, 20	170	Type II	228
CoZnAl-LDH/rGO/g-C_3N_4	300 W Xe lamp	GP, $CO_2 + H_2O$	CO, 10.1	20.2	Z-Scheme	229
g-C_3N_4/Ag_3VO_4/rGO	Xe lamp	LP, aqueous solution of TEOA	CO, 7.03 CH_4, 1.40	25.3	Z-Scheme	230
g-C_3N_4/BiOI/rGO	300 W Xe lamp, 400 nm filter	GP, $CO_2 + H_2O$	CO, 2.73	5.46	Z-Scheme	231
ZnV_2O_6/rGO/g-C_3N_4	35 W Xe lamp, 20 mW cm^{-2}	LP, aqueous NaOH	CH_3OH, 543	3260	Z-Scheme	232

Note. NiAl-LDH are Ni and Al layered double hydroxides; CoZnAl-LDH are Co, Zn and Al layered double hydroxides.

CH_3OH formation rate on exposure to a xenon lamp was 630 μmol g^{-1} h^{-1}. Meanwhile, the CH_3OH formation rate in a reactor without external reflection was about 520 μmol g^{-1} h^{-1}. Thus, even without the use of reflected light energy, the obtained photocatalyst activity is quite high, which is attributable to implementation of the S-scheme between two narrow-band-gap semiconductors and to participation of rGO as a mediator for efficient photogenerated charge carrier separation.

Data on the photocatalysts based on rGO/g-C_3N_4 reported in recent years are summarized in Table 8.

Only ternary systems, mainly containing some type of vanadate or layered double hydroxide (LDH) as the third component, are considered here, because in the case of binary rGO/g-C_3N_4 photocatalysts, high CO_2 reduction rates are not attained. Layered double hydroxides are a group of layered solids formed by different-valence metal ions and hydroxide ions, which possess a lot of unique properties such as possibility of surface functionalization, intercalation of anions and high chemical stability; this makes LDHs promising photocatalytic materials.[233–235] Most experiments on CO_2 reduction catalyzed by rGO/g-C_3N_4-based photocatalysts were carried out in the liquid phase and the highest W_e values were found for ZnV_2O_6/rGO/g-C_3N_4 systems with Z-scheme charge transfer.

5. Conclusion

Development of g-C_3N_4-based photocatalysts for CO_2 reduction has been a significant research subject in recent years, which is confirmed by the steadily increasing number of relevant publications. The high interest of researchers in the g-C_3N_4-based photocatalysts is caused by unique properties of g-C_3N_4, mostly, narrow band gap, which allows activation by visible light. However, narrow-band-gap semiconductors are characterized by high recombination rate of photogenerated charge carriers. Other drawbacks of unmodified g-C_3N_4 are low adsorption capacity towards CO_2 and, as a rule, low specific surface area, which result in moderate rate of CO_2 reduction. Modification of g-C_3N_4 mitigates the effect of these drawbacks on the photocatalytic process; the fabrication of heterostructures with other semiconductors represents the most popular modification method, as it allows for the control of the properties of photocatalysts and the subsequent increase in the CO_2 reduction rate.

Currently g-C_3N_4 heterostructures with metal oxides and sulfides, MXenes, and rGO are the most studied composite photocatalysts based on g-C_3N_4. Among these materials, TiO_2 is mostly studied, because it is a traditional material for many photocatalytic applications owing to its ready availability, lack of toxicity and stability. One more promising oxide semiconductor is CeO_2 owing to its unique feature, that is, change in the cerium oxidation state, giving rise to electron traps and additional adsorption sites. MXenes are a new class of 2D compounds with promising properties for the formation of heterostructures and photocatalytic applications. Various approaches to MXene synthesis make it possible to vary their surface properties, which opens up the way for development of a broad range of photocatalysts. Partially reduced graphene oxide rGO has also gained popularity in recent years, and a great potential of rGO for the use in photocatalytic CO_2 reduction systems has already been shown.

It is worth mentioning that comparison of the current studies on the photocatalytic CO_2 reduction is difficult because no unified experimental methodology has yet been developed. Studies of similar photocatalysts under similar reaction conditions by different research groups often result in significant differences not only in the rates of product formation, but also in the set of products, which may probably be caused by incomplete removal of organic impurities from the reaction medium or by low level of experimentation. Nevertheless, even though establishing of a strict correlation is problematic, it is still possible to determine the average productivity of particular systems to identify the most promising photocatalysts. The results considered in the review provide the conclusion that TiO_2 is most promising among the traditional materials used in photocatalysis for the formation of heterostructures with g-C_3N_4; this provides W_e values at the level of 200–600 mmol g^{-1} h^{-1}, and in some cases, up to 6700 mmol g^{-1} h^{-1}. In addition, there is a persistent trend towards the use of 2D materials such as MXenes and rGO for the formation of heterostructures. Indeed, in some studies, fairly high CO_2 reduction rates have already been attained by using Ti_3C_2 or rGO to modify g-C_3N_4. The major products formed upon CO_2 reduction catalyzed by

heterostructures based on traditional semiconductors and those based on new 2D materials are CO and CH_4. However, in some cases, outstanding rates of CH_3OH formation have been achieved using rGO.

Thus, data on the activity of photocatalysts reported in the literature indicate that practical implementation of the photocatalytic CO_2 reduction requires much more active systems and, probably, the main trend of research in the photocatalytic CO_2 reduction for the next decade will be the search for and development of composite photocatalysts based on g-C_3N_4 combined with various 2D semiconductor materials and with materials (*e.g.*, bentonite) that may significantly improve the textural properties of composites.

This study was financially supported by the Russian Science Foundation (Project No. 21-73–10235).

6. List of acronyms

AQE — apparent quantum efficiency,
bpy — bipyridine,
CB — conduction band,
DETA — diethylenetriamine,
DMF — dimethylformamide,
g-C_3N_4 — graphitic carbon nitride,
GO — graphene oxide,
GP — gas phase,
LDH — layered double hydroxide,
LP — liquid phase,
m — mesoporous,
MXene — a class of two-dimensional metal carbides, nitrides or carbonitrides,
NHE — normal hydrogen electrode,
P-MWNT — pre-treated multi-walled carbon nanotubes,
PNS — porous nanosheets,
rGO — partially reduced graphene oxide,
SC — semiconductor,
TEOA — triethanolamine,
VB — valence band,
W_e — total number of electrons consumed in a photocatalytic process per unit reaction time and per unit photocatalyst mass.

7. References

1. P.Acharya, R.Ghimire, W.S.Paye, A.C.Ganguli, S.J.DelGrosso. *Sci. Rep.*, **12**, 1 (2022); https://doi.org/10.1038/s41598-022-16719-w
2. J.Wang, W.Azam. *Geosci. Front.*, **15**, 101757 (2024); https://doi.org/10.1016/j.gsf.2023.101757
3. Y.Li, M.Zhou, B.Cheng, Y.Shao. *J. Mater. Sci. Technol.*, **56**, 1 (2020); https://doi.org/10.1016/J.JMST.2020.04.028
4. A.L.Maximov, I.P.Beletskaya. *Russ. Chem. Rev.*, **93** (1), RCR5101 (2024); https://doi.org/10.59761/rcr5101
5. K.C.Christoforidis, P.Fornasiero. *ChemCatChem*, **11**, 368 (2019); https://doi.org/10.1002/CCTC.201801198
6. P.R.Yaashikaa, P.Senthil Kumar, S.J.Varjani, A.Saravanan. *J. CO_2 Util.*, **33**, 131 (2019); https://doi.org/10.1016/J.JCOU.2019.05.017
7. A.A.Saraev, A.Y.Kurenkova, E.Y.Gerasimov, E.A.Kozlova. *Nanomaterials*, **12**, 1584 (2022); https://doi.org/10.3390/NANO12091584
8. A.V.Kuzmin, B.A.Shainyan. *Russ. Chem. Rev.*, **92** (6), RCR5085 (2023); https://doi.org/10.59761/RCR5085
9. E.Alper, O.Yuksel Orhan. *Petroleum*, **3**, 109 (2017); https://doi.org/10.1016/J.PETLM.2016.11.003
10. A.Saravanan, P.Senthil kumar, D.-V.N.Vo, S.Jeevanantham, V.Bhuvaneswari, V.Anantha Narayanan, P.R.Yaashikaa, S.Swetha, B.Reshma. *Chem. Eng. Sci.*, **236**, 116515 (2021); https://doi.org/10.1016/J.CES.2021.116515
11. J.Ma, N.Sun, X.Zhang, N.Zhao, F.Xiao, W.Wei, Y.Sun. *Catal. Today*, **148**, 221 (2009); https://doi.org/10.1016/J.CATTOD.2009.08.015
12. E.A.Kozlova, M.N.Lyulyukin, D.V.Kozlov, V.N.Parmon. *Russ. Chem. Rev.*, **90**, 1520 (2021); https://doi.org/10.1070/rcr5004
13. S.S.Meryem, S.Nasreen, M.Siddique, R.Khan. *Rev. Chem. Eng.*, **34**, 409 (2018); https://doi.org/10.1515/REVCE-2016-0016
14. S.Xu, E.A.Carter. *Chem. Rev*., **119**, 6631 (2019); https://doi.org/10.1021/acs.chemrev.8b00481
15. Y.Matsubara, D.C.Grills, Y.Kuwahara. *ACS Catal.*, **5**, 6440 (2015); https://doi.org/10.1021/acscatal.5b00656
16. N.Shehzad, M.Tahir, K.Johari, T.Murugesan, M.Hussain. *J. CO_2 Util.*, **26**, 98 (2018); https://doi.org/10.1016/j.jcou.2018.04.026
17. S.G.Zlotin, K.S.Egorova, V.P.Ananikov, A.A.Akulov, M.V.Varaksin, O.N.Chupakhin, V.N.Charushin, K.P.Bryliakov, A.D.Averin, I.P.Beletskaya, E.L.Dolengovski, Y.H.Budnikova, O.G.Sinyashin, Z.N.Gafurov, A.O.Kantyukov, D.G.Yakhvarov, A.V.Aksenov, M.N.Elinson, V.G.Nenajdenko, A.M.Chibiryaev, N.S.Nesterov, E.A.Kozlova, O.N.Martyanov, I.A.Balova, V.N.Sorokoumov, D.A.Guk, E.K.Beloglazkina, D.A.Lemenovskii, I.Y.Chukicheva, L.L.Frolova, E.S.Izmest'ev, I.A.Dvornikova, A.V.Popov, A.V.Kutchin, D.M.Borisova, A.A.Kalinina, A.M.Muzafarov, I.V.Kuchurov, A.L.Maximov, A.V.Zolotukhina. *Russ. Chem. Rev.*, **92** (12), RCR5104, (2023); https://doi.org/10.59761/RCR5104
18. B.Dam, B.Das, B.K.Patel. *Green Chem.*, **25**, 3374 (2023); https://doi.org/10.1039/D3GC00669G
19. A.Alaghmandfard, K.Ghandi. *Nanomaterials*, **12**, 294 (2022); https://doi.org/10.3390/NANO12020294
20. F.Kessler, Y.Zheng, D.Schwarz, C.Merschjann, W.Schnick, X.Wang, M.J.Bojdys. *Nat. Rev. Mater.*, **2**, 17030 (2017); https://doi.org/10.1038/natrevmats.2017.30
21. X.Zhang, S.P.Jiang. *Mater. Today Energy*, **23**, 100904 (2022); https://doi.org/10.1016/j.mtener.2021.100904
22. W.J.Ong, L.L.Tan, Y.H.Ng, S.T.Yong, S.P.Chai. *Chem. Rev.*, **116**, 7159 (2016); https://doi.org/10.1021/acs.chemrev.6b00075
23. Y.Zhang, Z.Zhou, Y.Zhang, Y.Shen, S.Liu. *Chem. Soc. Rev.*, **47**, 2298 (2018); https://doi.org/10.1039/c7cs00840f
24. L.A.Lebedev, M.I.Chebanenko, E.V.Dzhevaga, K.D.Martinson, V.I.Popkov. *Mendeleev Commun.*, **32**, 317 (2022); https://doi.org/10.1016/j.mencom.2022.05.008
25. F.R.Fan, R.Wang, H.Zhang, W.Wu. *Chem. Soc. Rev.*, **50**, 10983 (2021); https://doi.org/10.1039/C9CS00821G
26. D.Liu, A.Barbar, T.Najam, M.S.Javed, J.Shen, P.Tsiakaras, X.Cai. *Appl. Catal. B: Environ.*, **297**, 120389 (2021); https://doi.org/10.1016/J.APCATB.2021.120389
27. W.K.Darkwah, K.A.Oswald. *Nanoscale Res. Lett.*, **14**, 234 (2019); https://doi.org/10.1186/s11671-019-3070-3
28. B.Zhu, S.Wageh, A.A.Al-Ghamdi, S.Yang, Z.Tian, J.Yu. *Catal. Today*, **335**, 117 (2019); https://doi.org/10.1016/J.CATTOD.2018.09.038
29. B.Zhu, L.Zhang, D.Xu, B.Cheng, J.Yu. *J. CO_2 Util.*, **21**, 327 (2017); https://doi.org/10.1016/J.JCOU.2017.07.021
30. K.Zhang, M.Zhou, C.Yu, K.Yang, X.Li, W.Dai, J.Guan, Q.Shu, W.Huang. *Dyes Pigments.*, **180**, 108525 (2020); https://doi.org/10.1016/J.DYEPIG.2020.108525
31. X.Zhang, Y.Zhang, X.Jia, N.Zhang, R.Xia, X.Zhang, Z.Wang, M.Yu. *Sep. Purif. Technol.*, **268**, 118691 (2021); https://doi.org/10.1016/J.SEPPUR.2021.118691
32. Y.Huo, J.Zhang, K.Dai, C.Liang. *ACS Appl. Energy Mater.*, **4**, 956 (2021); https://doi.org/10.1021/ACSAEM.0C02896

33. P.Hao, Z.Chen, Y.Yan, W.Shi, F.Guo. *Sep. Purif. Technol.*, **330**, 125302 (2024); https://doi.org/10.1016/j.seppur.2023.125302
34. A.Hezam, T.Peppel, J.Strunk. *Curr. Opin. Green Sustain. Chem.*, **41**, 100789 (2023); https://doi.org/10.1016/J.COGSC.2023.100789
35. Y.Li, Z.Xia, Q.Yang, L.Wang, Y.Xing. *J. Mater. Sci. Technol.*, **125**, 128 (2022); https://doi.org/10.1016/j.jmst.2022.02.035
36. J.Li, H.Yuan, W.Zhang, B.Jin, Q.Feng, J.Huang, Z.Jiao. *Carbon Energy*, **4**, 294 (2022); https://doi.org/10.1002/CEY2.179
37. J.Lin, W.Tian, H.Zhang, X.Duan, H.Sun, S.Wang. *Energy Fuels*, **35**, 7 (2021); https://doi.org/10.1021/ACS.ENERGYFUELS.0C03048
38. G.Liao, C.Li, X.Li, B.Fang. *Cell Reports Phys. Sci.*, **2**, 100355 (2021); https://doi.org/10.1016/j.xcrp.2021.100355
39. J.Tauc, R.Grigorovici, A.Vancu. *Phys. Stat. Sol.*, **15**, 627, (1966); https://doi.org/10.1002/pssb.19660150224
40. P.Makuła, M.Pacia, W.Macyk. *J. Phys. Chem. Lett.*, **9**, 6814 (2018); https://doi.org/10.1021/acs.jpclett.8b02892
41. H.Ou, X.Chen, L.Lin, Y.Fang, X.Wang. *Angew. Chem., Int. Ed.*, **57**, 8729 (2018); https://doi.org/10.1002/ANIE.201803863
42. J.Jing, Z.Chen, C.Feng. *Electrochim. Acta*, **297**, 488 (2019); https://doi.org/10.1016/j.electacta.2018.12.015
43. Y.Fang, Y.Xu, X.Li, Y.Ma, X.Wang. *Angew. Chem., Int. Ed.*, **57**, 9749 (2018); https://doi.org/10.1002/ANIE.201804530
44. J.Jing, Z.Chen, C.Feng, M.Sun, J.Hou. *J. Alloys Compd.*, **851**, 156820 (2021); https://doi.org/10.1016/J.JALLCOM.2020.156820
45. E.Wierzyńska, M.Pisarek, T.Łęcki, M.Skompska. *Molecules*, **28**, 2469 (2023); https://doi.org/10.3390/MOLECULES28062469
46. F.Cheng, H.Wang, X.Dong. *Chem. Commun.*, **51**, 7176 (2015); https://doi.org/10.1039/C5CC01035G
47. Y.Zhang, M.Antonietti. *Chem. Asian J.*, **5**, 1307 (2010); https://doi.org/10.1002/ASIA.200900685
48. J.Luo, G.Dong, Y.Zhu, Z.Yang, C.Wang. *Appl. Catal. B: Environ.*, **214**, 46 (2017); https://doi.org/10.1016/J.APCATB.2017.05.016
49. S.Ye, R.Wang, M.Z.Wu, Y.P.Yuan. *Appl. Surf. Sci.*, **358**, 15 (2015); https://doi.org/10.1016/J.APSUSC.2015.08.173
50. K.R.Reddy, C.V.Reddy, M.N.Nadagouda, N.P.Shetti, S.Jaesool, T.M.Aminabhavi. *J. Environ. Manag.*, **238**, 25 (2019); https://doi.org/10.1016/J.JENVMAN.2019.02.075
51. S.Cao, J.Low, J.Yu, M.Jaroniec. *Adv. Mater.*, **27**, 2150 (2015); https://doi.org/10.1002/ADMA.201500033
52. Z.Lin, X.Wang. *Angew. Chem., Int. Ed.*, **52**, 1735 (2013); https://doi.org/10.1002/ANIE.201209017
53. Z.Yang, Y.Zhang, Z.Schnepp. *J. Mater. Chem. A*, **3**, 14081 (2015); https://doi.org/10.1039/C5TA02156A
54. J.Wang, S.Wang. *Coord. Chem. Rev.*, **453**, 214338 (2022); https://doi.org/10.1016/J.CCR.2021.214338
55. S.M.Abu-Sari, W.M.A.W.Daud, M.F.A.Patah, B.C.Ang. *Adv. Colloid Interface Sci.*, **307**, 102722 (2022); https://doi.org/10.1016/J.CIS.2022.102722
56. M.Inagaki, T.Tsumura, T.Kinumoto, M.Toyoda. *Carbon*, **141**, 580 (2019); https://doi.org/10.1016/J.CARBON.2018.09.082
57. H.Huang, L.Jiang, J.Yang, S.Zhou, X.Yuan, J.Liang, H.Wang, H.Wang, Y.Bu, H.Li. *Renew. Sustain. Energy Rev.*, **173**, 113110 (2023); https://doi.org/10.1016/J.RSER.2022.113110
58. Q.Wang, Z.Fang, W.Zhang, D.Zhang. *Adv. Fiber Mater*, **4**, 342 (2022); https://doi.org/10.1007/S42765-021-00122-7
59. Y.Li, M.Zhang, L.Zhou, S.Yang, Z.Wu, Y.Ma. *Wuli Huaxue Xuebao/ Acta Phys. – Chim. Sin.*, **37**, 2009030 (2021); https://doi.org/10.3866/PKU.WHXB202009030
60. Q.Xu, Z.Xia, J.Zhang, Z.Wei, Q.Guo, H.Jin, H.Tang, S.Li, X.Pan, Z.Su, S.Wang. *Carbon Energy*, **5**, e205 (2023); https://doi.org/10.1002/CEY2.205
61. U.Ghosh, A.Majumdar, A.Pal. *J. Environ. Chem. Eng.*, **9**, 104631 (2021); https://doi.org/10.1016/j.jece.2020.104631
62. B.He, Y.Cui, Y.Lei, W.Li, J.Sun. *J. Colloid Interface Sci.*, **629**, 825 (2023); https://doi.org/10.1016/J.JCIS.2022.09.114
63. M.Aggarwal, S.Basu, N.P.Shetti, M.N.Nadagouda, E.E.Kwon, Y.K.Park, T.M.Aminabhavi. *Chem. Eng. J.*, **425**, 131402 (2021); https://doi.org/10.1016/J.CEJ.2021.131402
64. C.Prasad, N.Madkhali, V.Govinda, H.Y.Choi, I.Bahadur, S.Sangaraju. *J. Environ. Chem. Eng.*, **11**, 109727 (2023); https://doi.org/10.1016/J.JECE.2023.109727
65. M.Zhang, Y.Yang, X.An, L.-an Hou. *Chem. Eng. J.*, **412**, 128663 (2021); https://doi.org/10.1016/J.CEJ.2021.128663
66. X.Liu, R.Ma, L.Zhuang, B.Hu, J.Chen, X.Liu, X.Wang. *Crit. Rev. Environ. Sci. Technol.*, **51**, 751 (2021); https://doi.org/10.1080/10643389.2020.1734433
67. N.Sun, Y.Zhu, M.Li, J.Zhang, J.Qin, Y.Li, C.Wang. *Appl. Catal. B: Environ.*, **298**, 120565 (2021); https://doi.org/10.1016/j.apcatb.2021.120565
68. A.Y.Kurenkova, E.Y.Gerasimov, A.A.Saraev, E.A.Kozlova. *Russ. Chem. Bull.*, **72**, 269 (2023); https://doi.org/10.1007/s11172-023-3732-2
69. R.Kavitha, P.M.Nithya, S.Girish Kumar. *Appl. Surf. Sci.*, **508**, 145142 (2020); https://doi.org/10.1016/j.apsusc.2019.145142
70. A.A.Saraev, A.Y.Kurenkova, A.V.Zhurenok, E.Y.Gerasimov, E.A.Kozlova. *Catalysts*, **13**, 273 (2023); https://doi.org/10.3390/catal13020273
71. A.V.Zhurenok, D.B.Vasilchenko, E.A.Kozlova. *Int. J. Mol. Sci.*, **24**, 346 (2023); https://doi.org/10.3390/ijms24010346
72. A.L.Linsebigler, G.Lu, J.T.Yates. *Chem. Rev.*, **95**, 735 (1995); https://doi.org/10.1021/cr00035a013
73. A.A.Rempel, A.A.Valeeva, A.S.Vokhmintsev, I.A.Weinstein. *Russ. Chem. Rev.*, **90**, 1397 (2021); https://doi.org/10.1070/RCR4991
74. A.A.Valeeva, A.A.Rempel, S.V.Rempel, S.I.Sadovnikov, A.I.Gusev. *Russ. Chem. Rev.*, **90**, 601 (2021); https://doi.org/10.1070/RCR4967/XML
75. H.Abdullah, M.R.Khan, M.Pudukudy, Z.Yaakob, N.A.Ismail. *J. Rare Earths*, **33**, 1155 (2015); https://doi.org/10.1016/S1002-0721(14)60540-8
76. X.Li, J.Yu, J.Low, Y.Fang, J.Xiao, X.Chen. *J. Mater. Chem. A*, **3**, 2485 (2015); https://doi.org/10.1039/c4ta04461d
77. A.Sewnet, M.Abebe, P.Asaithambi, E.Alemayehu. *Air Soil Water Res.*, **15**, (2022); https://doi.org/10.1177/11786221221117266
78. R.Acharya, K.Parida. *J. Environ. Chem. Eng.*, **8**, 103896 (2020); https://doi.org/10.1016/J.JECE.2020.103896
79. J.Zhang, P.Zhou, J.Liu, J.Yu. *Phys. Chem. Chem. Phys.*, **16**, 20382 (2014); https://doi.org/10.1039/C4CP02201G
80. A.I.Gopalan, J.C.Lee, G.Saianand, K.P.Lee, P.Sonar, R.Dharmarajan, Y.L.Hou, K.Y.Ann, V.Kannan, W.J.Kim. *Nanomaterials*, **10**, 1854 (2020); https://doi.org/10.3390/NANO10091854
81. D.M.Tobaldi, R.C.Pullar, A.F.Gualtieri, M.P.Seabra, J.A.Labrincha. *Chem. Eng. J.*, **214**, 364 (2013); https://doi.org/10.1016/J.CEJ.2012.11.018
82. R.Daghrir, P.Drogui, D.Robert. *Ind. Eng. Chem. Res.*, **52**, 3581 (2013); https://doi.org/10.1021/IE303468T
83. G.Song, C.Luo, Q.Fu, C.Pan. *RSC Adv.*, **6**, 84035 (2016); https://doi.org/10.1039/C6RA17665H
84. X.Q.Gong, A.Selloni. *J. Phys. Chem. B*, **109**, 19560 (2005); https://doi.org/10.1021/JP055311G
85. C.Jia, T.Dong, M.Li, P.Wang, P.Yang. *J. Alloys Compd.*, **769**, 521 (2018); https://doi.org/10.1016/J.JALLCOM.2018.08.035
86. L.Zhou, L.Wang, J.Zhang, J.Lei, Y.Liu. *Res. Chem. Intermed.*, **43**, 2081 (2017); https://doi.org/10.1007/s11164-016-2748-8
87. S.Mehregan, F.Hayati, M.Mehregan, A.A.Isari, A.Jonidi Jafari, S.Giannakis, B.Kakavandi. *Environ. Sci. Pollut. Res.*, **29**, 74951 (2022); https://doi.org/10.1007/S11356-022-21048-6
88. S.Ahmed, M.G.Rasul, R.Brown, M.A.Hashib. *J. Environ. Manag.*, **92**, 311 (2011); https://doi.org/10.1016/J.JENVMAN.2010.08.028

89. M.Mahalakshmi, B.Arabindoo, M.Palanichamy, V.Murugesan. *J. Hazard. Mater.*, **143**, 240 (2007); https://doi.org/10.1016/J.JHAZMAT.2006.09.008
90. B.Ohtani, O.O.Prieto-Mahaney, D.Li, R.Abe. *J. Photochem. Photobiol. A: Chem.*, **216**, 179 (2010); https://doi.org/10.1016/J.JPHOTOCHEM.2010.07.024
91. H.Wang, H.Li, Z.Chen, J.Li, X.Li, P.Huo, Q.Wang. *Solid State Sci.*, **100**, 106099 (2020); https://doi.org/10.1016/J.SOLIDSTATESCIENCES.2019.106099
92. N.T.Thanh Truc, L.Giang Bach, N.Thi Hanh, T.D.Pham, N.Thi Phuong Le Chi, D.T.Tran, M.V.Nguyen, V.N.Nguyen. *J. Colloid Interface Sci.*, **540**, 1 (2019); https://doi.org/10.1016/J.JCIS.2019.01.005
93. R.Zhong, Y.Liang, F.Huang, S.Liang, S.Liu. *Chinese J. Catal.*, **53**, 109 (2023); https://doi.org/10.1016/S1872-2067(23)64513-9
94. F.Capasso. *Science*, **235**, 172 (1987); https://doi.org/10.1126/SCIENCE.235.4785.172
95. G.Zhang, G.Kim, W.Choi. *Energy Environ. Sci.*, **7**, 954 (2014); https://doi.org/10.1039/c3ee43147a
96. T.Cottineau, N.Béalu, P.A.Gross, S.N.Pronkin, N.Keller, E.R.Savinova, V.Keller. *J. Mater. Chem. A*, **1**, 2151 (2013); https://doi.org/10.1039/C2TA00922F
97. R.B.P.Marcelino, C.C.Amorim. *Environ. Sci. Pollut. Res.*, **26**, 4155 (2019); https://doi.org/10.1007/S11356-018-3117-5
98. K.Li, B.Peng, T.Peng. *ACS Catal.*, **6**, 7485 (2016); https://doi.org/10.1021/ACSCATAL.6B02089
99. L.Wang, B.Zhao, C.Wang, M.Sun, Y.Yu, B.Zhang. *J. Mater. Chem. A*, **8**, 10175 (2020); https://doi.org/10.1039/D0TA01256D
100. X.Jiang, J.Huang, Z.Bi, W.Ni, G.Gurzadyan, Y.Zhu, Z.Zhang. *Adv. Mater.*, **34**, 2109330 (2022); https://doi.org/10.1002/ADMA.202109330
101. K.Li, B.Peng, J.Jin, L.Zan, T.Peng. *Appl. Catal. B: Environ.*, **203**, 910 (2017); https://doi.org/10.1016/J.APCATB.2016.11.001
102. H.Zhang, H.Bian, F.Wang, L.Zhu, S.Zhang, D.Xia. *Colloids Surfaces A: Physicochem. Eng. Asp.*, **674**, 131989 (2023); https://doi.org/10.1016/j.colsurfa.2023.131989
103. A.Banitalebi Dehkordi, A.Ziarati, J.B.Ghasemi, A.Badiei. *Sol. Energy*, **205**, 465 (2020); https://doi.org/10.1016/J.SOLENER.2020.05.071
104. C.Wang, Y.Zhao, H.Xu, Y.Li, Y.Wei, J.Liu, Z.Zhao. *Appl. Catal. B: Environ.*, **263**, 118314 (2020); https://doi.org/10.1016/J.APCATB.2019.118314
105. M.Chen, J.Wu, C.Lu, X.Luo, Y.Huang, B.Jin, H.Gao, X.Zhang, M.Argyle, Z.Liang. *Green Energy Environ.*, **6**, 938 (2021); https://doi.org/10.1016/J.GEE.2020.07.001
106. Q.Wang, L.Zhang, Y.Guo, M.Shen, M.Wang, B.Li, J.Shi. *Chem. Eng. J.*, **396**, 125347 (2020); https://doi.org/10.1016/J.CEJ.2020.125347
107. H.Shi, J.Du, J.Hou, W.Ni, C.Song, K.Li, G.G.Gurzadyan, X.Guo. *J. CO_2 Util.*, **38**, 16 (2020); https://doi.org/10.1016/J.JCOU.2020.01.005
108. F.He, B.Zhu, B.Cheng, J.Yu, W.Ho, W.Macyk. *Appl. Catal. B: Environ.*, **272**, 119006 (2020); https://doi.org/10.1016/J.APCATB.2020.119006
109. D.P.Kumar, A.P.Rangappa, H.S.Shim, K.H.Do, Y.Hong, M.Gopannagari, K.A.J.Reddy, P.Bhavani, D.A.Reddy, J.K.Song, T.K.Kim. *Mater. Today Chem.*, **24**, 100827 (2022); https://doi.org/10.1016/J.MTCHEM.2022.100827
110. M.H.Foghani, O.Tavakoli, M.J.Parnian, R.Zarghami. *Chem. Pap.*, **76**, 3459 (2022); https://doi.org/10.1007/S11696-022-02109-Z
111. L.Hammoud, C.Marchal, C.Colbeau-Justin, J.Toufaily, T.Hamieh, V.Caps, V.Keller. *Energy Technol.*, **11**, 2201363 (2023); https://doi.org/10.1002/ENTE.202201363
112. S.Cheng, Z.Sun, K.H.Lim, K.Liu, A.A.Wibowo, T.Du, L.Liu, H.T.Nguyen, G.K.Li, Z.Yin, S.Kawi. *Appl. Catal. B: Environ.*, **343**, 123583 (2024); https://doi.org/10.1016/j.apcatb.2023.123583
113. Y.Wang, X.Xiao, H.Xue, H.Pang. *ChemistrySelect*, **3**, 550 (2018); https://doi.org/10.1002/slct.201702780
114. T.Ringu, S.Ghosh, A.Das, N.Pramanik. *Emergent Mater.*, **5**, 1629 (2022); https://doi.org/10.1007/s42247-022-00402-x
115. M.Ding, Z.Guo, L.Zhou, X.Fang, L.Zhang, L.Zeng, L.Xie, H.Zhao. *Crystals,* **8**, 223 (2018); https://doi.org/10.3390/CRYST8050223
116. M.Nemiwal, T.C.Zhang, D.Kumar. *Sci. Total Environ.*, **767**, 144896 (2021); https://doi.org/10.1016/J.SCITOTENV.2020.144896
117. J.Kaupužs, A.Medvids, P.Onufrijevs, H.Mimura. *Opt. Laser Technol.*, **111**, 121 (2019); https://doi.org/10.1016/j.optlastec.2018.09.037
118. C.Chen, J.Jin, S.Chen, T.Wang, J.Xiao, T.Peng. *Mater. Res. Bull.*, **137**, 111177 (2021); https://doi.org/10.1016/J.MATERRESBULL.2020.111177
119. Q.Guo, L.Fu, T.Yan, W.Tian, D.Ma, J.Li, Y.Jiang, X.Wang. *Appl. Surf. Sci.*, **509**, 144773 (2020); https://doi.org/10.1016/j.apsusc.2019.144773
120. B.Liu, X.Zhao, C.Terashima, A.Fujishima, K.Nakata. *Phys. Chem. Chem. Phys.*, **16**, 8751 (2014); https://doi.org/10.1039/c3cp55317e
121. J.Albero, H.Garcia, A.Corma. *Top. Catal.*, **59**, 787 (2016); https://doi.org/10.1007/S11244-016-0550-X
122. L.L.Tan, W.J.Ong, S.P.Chai, A.R.Mohamed. *Chem. Eng. J.*, **308**, 248 (2017); https://doi.org/10.1016/J.CEJ.2016.09.050
123. Z.Zhu, C.Y.Chen, R.J.Wu. *J. Chinese Chem. Soc.*, **67**, 1654 (2020); https://doi.org/10.1002/JCCS.202000173
124. M.Sayed, B.Zhu, P.Kuang, X.Liu, B.Cheng, A.A.Al Ghamdi, S.Wageh, L.Zhang, J.Yu. *Adv. Sustain. Syst.*, **6**, 2100264 (2022); https://doi.org/10.1002/ADSU.202100264
125. U.Arif, F.Ali, A.Bahader, S.Ali, A.Zada, F.Raziq. *Inorg. Chem. Commun.*, **145**, 109944 (2022); https://doi.org/10.1016/J.INOCHE.2022.109944
126. J.Li, Y.Wang, Y.Wang, Y.Guo, S.Zhang, H.Song, X.Li, Q.Gao, W.Shang, S.Hu, H.Zheng, X.Li. *Nano Mater. Sci.*, **5**, 237 (2023); https://doi.org/10.1016/J.NANOMS.2023.02.003
127. T.H.Pham, M.H.Tran, T.T.H.Chu, Y.Myung, S.H.Jung, M.G.Mapari, K.Taeyoung. *Environ. Res.*, **217**, 114825 (2023); https://doi.org/10.1016/J.ENVRES.2022.114825
128. A.Bumajdad, J.Eastoe, A.Mathew. *Adv. Colloid Interface Sci.*, **147**–**148**, 56 (2009); https://doi.org/10.1016/J.CIS.2008.10.004
129. A.A.Fauzi, A.A.Jalil, N.S.Hassan, F.F.A.Aziz, M.S.Azami, I.Hussain, R.Saravanan, D.V.N.Vo. *Chemosphere*, **286**, 131651 (2022); https://doi.org/10.1016/J.CHEMOSPHERE.2021.131651
130. M.V.Erpalov, A.P.Tarutin, N.A.Danilov, D.A.Osinkin, D.A.Medvedev. *Russ. Chem. Rev.*, **92** (10), RCR5097 (2023); https://doi.org/10.59761/RCR5097
131. D.P.H.Tran, M.T.Pham, X.T.Bui, Y.F.Wang, S.J.You. *Sol. Energy*, **240**, 443 (2022); https://doi.org/10.1016/j.solener.2022.04.051
132. S.Sultana, S.Mansingh, K.M.Parida. *Mater. Adv.*, **2**, 6942 (2021); https://doi.org/10.1039/d1ma00539a
133. M.Liang, T.Borjigin, Y.Zhang, B.Liu, H.Liu, H.Guo. *Appl. Catal. B: Environ.*, **243**, 566 (2019); https://doi.org/10.1016/J.APCATB.2018.11.010
134. S.Fang, M.Rahaman, J.Bharti, E.Reisner, M.Robert, G.A.Ozin, Y.H.Hu. *Nat. Rev. Methods Primers*, **3**, 61 (2023); https://doi.org/10.1038/s43586-023-00243-w
135. C.C.Nguyen, N.N.Vu, T.O.Do. *J. Mater. Chem. A*, **3**, 18345 (2015); https://doi.org/10.1039/C5TA04326C
136. D.Wang, C.Miao, H.Li, B.Yu, W.Wang, Y.Wang, G.Che, C.Liu, B.Hu. *Mater. Res. Bull.*, **170**, 112552 (2024); https://doi.org/10.1016/J.MATERRESBULL.2023.112552
137. X.Li, J.Guan, H.Jiang, X.Song, P.Huo, H.Wang. *Appl. Surf. Sci.*, **563**, 150042 (2021); https://doi.org/10.1016/J.APSUSC.2021.150042
138. R.Tarcan, O.Todor-Boer, I.Petrovai, C.Leordean, S.Astilean, I.Botiz. *J. Mater. Chem. C*, **8**, 1198 (2020); https://doi.org/10.1039/c9tc04916a

139. X.Li, D.Shen, C.Liu, J.Li, Y.Zhou, X.Song, P.Huo, H.Wang, Y.Yan. *J. Colloid Interface Sci.*, **554**, 468 (2019); https://doi.org/10.1016/J.JCIS.2019.07.027
140. X.Zhao, J.Guan, J.Li, X.Li, H.Wang, P.Huo, Y.Yan. *Appl. Surf. Sci.*, **537**, 147891 (2021); https://doi.org/10.1016/J.APSUSC.2020.147891
141. H.Wang, J.Guan, J.Li, X.Li, C.Ma, P.Huo, Y.Yan. *Appl. Surf. Sci.*, **506**, 144931 (2020); https://doi.org/10.1016/J.APSUSC.2019.144931
142. W.Li, L.Jin, F.Gao, H.Wan, Y.Pu, X.Wei, C.Chen, W.Zou, C.Zhu, L.Dong. *Appl. Catal. B: Environ.*, **294**, 120257 (2021); https://doi.org/10.1016/J.APCATB.2021.120257
143. J.Chen, Y.Xiao, N.Wang, X.Kang, D.Wang, C.Wang, J.Liu, Y.Jiang, H.Fu. *Sci. China Mater.*, **66**, 3165 (2023); https://doi.org/10.1007/S40843-023-2443-0
144. H.Jiang, X.Li, S.Chen, H.Wang, P.Huo. *J. Mater. Sci.: Mater. Electron.*, **31**, 20495 (2020); https://doi.org/10.1007/S10854-020-04568-0
145. H.Hu, J.Hu, X.Wang, J.Gan, M.Su, W.Ye, W.Zhang, X.Ma, H.Wang. *Catal. Sci. Technol.*, **10**, 4712 (2020); https://doi.org/10.1039/D0CY00395F
146. F.E.Osterloh. *Chem. Soc. Rev.*, **42**, 2294 (2013); https://doi.org/10.1039/C2CS35266D
147. J.Zhu, Z.Yin, D.Yang, T.Sun, H.Yu, H.E.Hoster, H.H.Hng, H.Zhang, Q.Yan. *Energy Environ. Sci.*, **6**, 987 (2013); https://doi.org/10.1039/C2EE24148J
148. M.Shekofteh-Gohari, A.Habibi-Yangjeh, M.Abitorabi, A.Rouhi. *Crit. Rev. Environ. Sci. Technol.*, **48**, 806 (2018); https://doi.org/10.1080/10643389.2018.1487227
149. Y.Zhang, A.Thomas, M.Antonietti, X.Wang. *J. Am. Chem. Soc.*, **131**, 50 (2009); https://doi.org/10.1021/JA808329F
150. H.Kisch. *Angew. Chem., Int. Ed.*, **52**, 812 (2013); https://doi.org/10.1002/ANIE.201201200
151. D.Zhu, Q.Zhou. *Environ. Nanotechnol. Monit. Manag.*, **12**, 100255 (2019); https://doi.org/10.1016/J.ENMM.2019.100255
152. H.Guo, M.Chen, Q.Zhong, Y.Wang, W.Ma, J.Ding. *J. CO_2 Util.*, **33**, 233 (2019); https://doi.org/10.1016/J.JCOU.2019.05.016
153. B.Duan, L.Mei. *J. Colloid Interface Sci.*, **575**, 265 (2020); https://doi.org/10.1016/J.JCIS.2020.04.112
154. J.Lin, B.Qin, G.Zhao. *J. Photochem. Photobiol. A: Chem.*, **354**, 181 (2018); https://doi.org/10.1016/j.jphotochem.2017.09.019
155. P.V.Kamat, S.Jin. *ACS Energy Lett.*, **3**, 622 (2018); https://doi.org/10.1021/ACSENERGYLETT.8B00196
156. A.S.Hainer, J.S.Hodgins, V.Sandre, M.Vallieres, A.E.Lanterna, J.C.Scaiano. *ACS Energy Lett.*, **3**, 542 (2018); https://doi.org/10.1021/ACSENERGYLETT.8B00152
157. P.Christopher, S.Jin, K.Sivula, P.V.Kamat. *ACS Energy Lett.*, **6**, 707 (2021); https://doi.org/10.1021/ACSENERGYLETT.1C00064
158. R.Das, S.Chakraborty, S.C.Peter. *ACS Energy Lett.*, **6**, 3270 (2021); https://doi.org/10.1021/ACSENERGYLETT.1C01522
159. M.Padervand, S.Ghasemi, S.Hajiahmadi, C.Wang. *Appl. Surf. Sci.*, **544**, 148939 (2021); https://doi.org/10.1016/J.APSUSC.2021.148939
160. M.Padervand, B.Rhimi, C.Wang. *J. Alloys Compd.*, **852**, 156955 (2021); https://doi.org/10.1016/J.JALLCOM.2020.156955
161. Y.Shen, Q.Han, J.Hu, W.Gao, L.Wang, L.Yang, C.Gao, Q.Shen, C.Wu, X.Wang, X.Zhou, Y.Zhou, Z.Zou. *ACS Appl. Energy Mater.*, **3**, 6561 (2020); https://doi.org/10.1021/ACSAEM.0C00750
162. N.Bao, L.Shen, T.Takata, K.Domen. *Chem. Mater.*, **20**, 110 (2008); https://doi.org/10.1021/cm7029344
163. H.Yan, J.Yang, G.Ma, G.Wu, X.Zong, Z.Lei, J.Shi, C.Li. *J. Catal.*, **266**, 165 (2009); https://doi.org/10.1016/J.JCAT.2009.06.024
164. N.Bühler, K.Meier, J.F.Reber. *J. Phys. Chem.*, **88**, 3261 (1984); https://doi.org/10.1021/J150659A025
165. G.Ma, H.Yan, J.Shi, X.Zong, Z.Lei, C.Li. *J. Catal.*, **260**, 134 (2008); https://doi.org/10.1016/J.JCAT.2008.09.017
166. X.Ning, G.Lu. *Nanoscale*, **12**, 1213 (2020); https://doi.org/10.1039/C9NR09183A
167. D.J.Fermín, E.A.Ponomarev, L.M.Peter. *J. Electroanal. Chem.*, **473**, 192 (1999); https://doi.org/10.1016/S0022-0728(99)00109-6
168. Y.Chen, W.Zhong, F.Chen, P.Wang, J.Fan, H.Yu. *J. Mater. Sci. Technol.*, **121**, 19 (2022); https://doi.org/10.1016/J.JMST.2021.12.051
169. L.Wei, Z.Guo, X.Jia. *Catal. Lett.*, **151**, 56 (2021); https://doi.org/10.1007/S10562-020-03275-Z
170. N.N.Vu, S.Kaliaguine, T.O.Do. *ACS Appl. Energy Mater.*, **3**, 6422 (2020); https://doi.org/10.1021/ACSAEM.0C00656
171. H.Guo, J.Ding, S.Wan, Y.Wang, Q.Zhong. *Appl. Surf. Sci.*, **528**, 146943 (2020); https://doi.org/10.1016/j.apsusc.2020.146943
172. C.Zeng, H.Huang, T.Zhang, F.Dong, Y.Zhang, Y.Hu. *ACS Appl. Mater. Interfaces*, **9**, 27773 (2017); https://doi.org/10.1021/ACSAMI.7B08767
173. Y.Bai, L.Ye, T.Chen, P.Wang, L.Wang, X.Shi, P.K.Wong. *Appl. Catal. B: Environ.*, **203**, 633 (2017); https://doi.org/10.1016/J.APCATB.2016.10.066
174. J.Liang, Y.Chai, L.Li, D.Li, J.Shen, Y.Zhang, X.Wang. *Appl. Catal. B: Environ.*, **265**, 118551 (2020); https://doi.org/10.1016/J.APCATB.2019.118551
175. M.Gao, J.Yang, T.Sun, Z.Zhang, D.Zhang, H.Huang, H.Lin, Y.Fang, X.Wang. *Appl. Catal. B: Environ.*, **243**, 734 (2019); https://doi.org/10.1016/J.APCATB.2018.11.020
176. I.A.Mkhalid, R.M.Mohamed, A.A.Ismail, M.Alhaddad. *Ceram. Int.*, **47**, 17210 (2021); https://doi.org/10.1016/J.CERAMINT.2021.03.032
177. W.Ma, Y.Zhu, X.Wang. *J. Alloys Compd.*, **935**, 168129 (2023); https://doi.org/10.1016/J.JALLCOM.2022.168129
178. P.Madhusudan, R.Shi, S.Xiang, M.Jin, B.N.Chandrashekar, J.Wang, W.Wang, O.Peng, A.Amini, C.Cheng. *Appl. Catal. B: Environ.*, **282**, 119600 (2021); https://doi.org/10.1016/J.APCATB.2020.119600
179. J.Yu, C.Y.Xu, F.X.Ma, S.P.Hu, Y.W.Zhang, L.Zhen. *ACS Appl. Mater. Interfaces*, **6**, 22370 (2014); https://doi.org/10.1021/AM506396Z
180. Y.C.Zhang, Z.N.Du, K.W.Li, M.Zhang, D.D.Dionysiou. *ACS Appl. Mater. Interfaces*, **3**, 1528 (2011); https://doi.org/10.1021/AM200102Y
181. A.P.Rangappa, D.P.Kumar, J.Wang, K.H.Do, E.Kim, D.A.Reddy, H.S.Ahn, T.K.Kim. *J. Mater. Chem. A*, **10**, 7291 (2022); https://doi.org/10.1039/D1TA10463B
182. S.Yin, X.Zhao, E.Jiang, Y.Yan, P.Zhou, P.Huo. *Energy Environ. Sci.*, **15**, 1556 (2022); https://doi.org/10.1039/D1EE03764A
183. X.An, J.C.Yu, J.Tang. *J. Mater. Chem. A*, **2**, 1000 (2013); https://doi.org/10.1039/C3TA13846A
184. L.A.Burton, T.J.Whittles, D.Hesp, W.M.Linhart, J.M.Skelton, B.Hou, R.F.Webster, G.O'Dowd, C.Reece, D.Cherns, D.J.Fermin, T.D.Veal, V.R.Dhanak, A.Walsh. *J. Mater. Chem. A*, **4**, 1312 (2016); https://doi.org/10.1039/C5TA08214E
185. H.Wang, Z.Liu, L.Wang, Q.Shou, M.Gao, H.Wang, A.Nazir, P.Huo. *J. Mater. Sci.: Mater. Electron.*, **34**, 350 (2023); https://doi.org/10.1007/S10854-022-09642-3
186. S.Yin, L.Sun, Y.Zhou, X.Li, J.Li, X.Song, P.Huo, H.Wang, Y.Yan. *Chem. Eng. J.*, **406**, 126776 (2021); https://doi.org/10.1016/J.CEJ.2020.126776
187. Y.Huo, J.Zhang, K.Dai, Q.Li, J.Lv, G.Zhu, C.Liang. *Appl. Catal. B: Environ.*, **241**, 528 (2019); https://doi.org/10.1016/J.APCATB.2018.09.073
188. Y.Li, Q.Yin, Y.Zeng, Z.Liu. *Chem. Eng. J.*, **438**, 135652 (2022); https://doi.org/10.1016/J.CEJ.2022.135652
189. X.Chen, Y.Chen, X.Liu, Q.Wang, L.Li, L.Du, G.Tian. *Sci. China Mater.*, **65**, 400 (2022); https://doi.org/10.1007/S40843-021-1744-5
190. H.A.E.Omr, R.Putikam, M.K.Hussien, A.Sabbah, T.Y.Lin, K.H.Chen, H.L.Wu, S.P.Feng, M.C.Lin, H.Lee. *Appl.*

Catal. B: Environ., **324**, 122231 (2023); https://doi.org/10.1016/J.APCATB.2022.122231
191. H.A.E.Omr, R.Putikam, S.P.Feng, M.C.Lin, H.Lee. *Appl. Catal. B: Environ.*, **339**, 123103 (2023); https://doi.org/10.1016/J.APCATB.2023.123103
192. V.Talapatadur, S.S.Hegde, B.S.Surendra, P.Murahari, K.Ramesh. *Mater. Today Proc.*, (2023) (in the press); https://doi.org/10.1016/J.MATPR.2023.08.368
193. M.Naguib, M.Kurtoglu, V.Presser, J.Lu, J.Niu, M.Heon, L.Hultman, Y.Gogotsi, M.W.Barsoum. *Adv. Mater.*, **23**, 4248 (2011); https://doi.org/10.1002/ADMA.201102306
194. L.Cheng, X.Li, H.Zhang, Q.Xiang. *J. Phys. Chem. Lett.*, **10**, 3488 (2019); https://doi.org/10.1021/ACS.JPCLETT.9B00736
195. B.Anasori, M.R.Lukatskaya, Y.Gogotsi. *Nat. Rev. Mater.*, **2**, 16098 (2017); https://doi.org/10.1038/natrevmats.2016.98
196. Q.You, Zh.Guo, R.Zhang, Zh.Chang, M.Ge, Q.Mei, W.-F.Dong. *Sensors*, **21**, 3069 (2021); https://doi.org/10.3390/s21093069
197. X.Han, L.An, Y.Hu, Y.Li, C.Hou, H.Wang, Q.Zhang. *Appl. Catal. B; Environ.*, **265**, 118539 (2020); https://doi.org/10.1016/J.APCATB.2019.118539
198. J.Gonzalez-Julian. *J. Am. Ceram. Soc.*, **104**, 659 (2021); https://doi.org/10.1111/JACE.17544
199. S.W.Koh, L.Rekhi, N.Arramel, M.D.Birowosuto, Q.T.Trinh, J.Ge, W.Yu, A.T.S.Wee, T.S.Choksi, H.Li. *ACS Appl. Mater. Interfaces*, (2023) (in the press); https://doi.org/10.1021/acsami.3c11857
200. X.Li, Y.Bai, X.Shi, J.Huang, K.Zhang, R.Wang, L.Ye. *Appl. Surf. Sci.*, **546**, 149111 (2021); https://doi.org/10.1016/J.APSUSC.2021.149111
201. M.Tahir, B.Tahir. *Chem. Eng. J.*, **400**, 125868 (2020); https://doi.org/10.1016/J.CEJ.2020.125868
202. H.H.Murray. *Dev. Clay Sci.*, **2**, 111 (2006); https://doi.org/10.1016/S1572-4352(06)02006-X
203. I.H.Tseng, W.C.Chang, J.C.S.Wu. *Appl. Catal. B: Environ.*, **37**, 37 (2002); https://doi.org/10.1016/S0926-3373(01)00322-8
204. N.M.Dimitrijevic, B.K.Vijayan, O.G.Poluektov, T.Rajh, K.A.Gray, H.He, P.Zapol. *J. Am. Chem. Soc.*, **133**, 3964 (2011); https://doi.org/10.1021/JA108791U
205. Q.D.Truong, J.Y.Liu, C.C.Chung, Y.C.Ling. *Catal. Commun.*, **19**, 85 (2012); https://doi.org/10.1016/J.CATCOM.2011.12.025
206. K.Chandrasekaran, J.K.Thomas. *Chem. Phys. Lett.*, **99**, 7 (1983); https://doi.org/10.1016/0009-2614(83)80259-0
207. E.Karamian, S.Sharifnia. *J. CO_2 Util.*, **16**, 194 (2016); https://doi.org/10.1016/J.JCOU.2016.07.004
208. M.Madi, M.Tahir, Z.Y.Zakaria. *J. CO_2 Util.*, **65**, 102238 (2022); https://doi.org/10.1016/J.JCOU.2022.102238
209. Y.Guan, S.Jiang, Y.Cong, J.Wang, Z.Dong, Q.Zhang, G.Yuan, Y.Li, X.Li. *2D Materials*, **7**, 025010 (2020); https://doi.org/10.1088/2053-1583/AB6706
210. E.Ghasali, Y.Orooji, A.Azarniya, M.Alizadeh, M.Kazem-zad, TouradjEbadzadeh. *Appl. Surf. Sci.*, **542**, 148538 (2021); https://doi.org/10.1016/J.APSUSC.2020.148538
211. Y.Chen, H.Yao, F.Kong, H.Tian, G.Meng, S.Wang, X.Mao, X.Cui, X.Hou, J.Shi. *Appl. Catal. B: Environ.*, **297**, 120474 (2021); https://doi.org/10.1016/J.APCATB.2021.120474
212. Q.Shan, X.Mu, M.Alhabeb, C.E.Shuck, D.Pang, X.Zhao, X.F.Chu, Y.Wei, F.Du, G.Chen, Y.Gogotsi, Y.Gao, Y.Dall'Agnese. *Electrochem. Commun.*, **96**, 103 (2018); https://doi.org/10.1016/J.ELECOM.2018.10.012
213. C.Ling, L.Shi, Y.Ouyang, Q.Chen, J.Wang, C.Y.Ling, L.Shi, Y.X.Ouyang, Q.Chen, J.L.Wang. *Adv. Sci.*, **3**, 1600180 (2016); https://doi.org/10.1002/ADVS.201600180
214. C.Yang, Q.Tan, Q.Li, J.Zhou, J.Fan, B.Li, J.Sun, K.Lv. *Appl. Catal. B: Environ.*, **268**, 118738 (2020); https://doi.org/10.1016/j.apcatb.2020.118738
215. Q.Tang, Z.Sun, S.Deng, H.Wang, Z.Wu. *J. Colloid Interface Sci.*, **564**, 406 (2020); https://doi.org/10.1016/J.JCIS.2019.12.091
216. Y.Yang, D.Zhang, J.Fan, Y.Liao, Q.Xiang. *RRL Solar*, **5**, 2000351 (2021); https://doi.org/10.1002/SOLR.202000351
217. J.Hu, J.Ding, Q.Zhong. *J. Colloid Interface Sci.*, **582**, 647 (2021); https://doi.org/10.1016/J.JCIS.2020.08.047
218. H.Wang, Q.Tang, Z.Wu. *ACS Sustain. Chem. Eng.*, (2021); https://doi.org/10.1021/ACSSUSCHEMENG.1C01155
219. Y.H.Ng, A.Iwase, N.J.Bell, A.Kudo, R.Amal. *Catal. Today*, **164**, 353 (2011); https://doi.org/10.1016/J.CATTOD.2010.10.090
220. W.S.Hummers, R.E.Offeman. *J. Am. Chem. Soc.*, **80**, 1339 (1958); https://doi.org/10.1021/JA01539A017
221. A.N.Ghulam, O.A.L.Dos Santos, L.Hazeem, B.P.Backx, M.Bououdina, S.Bellucci. *J. Funct. Biomater.*, **13**, 77 (2022); https://doi.org/10.3390/JFB13020077
222. A.Mondal, A.Prabhakaran, S.Gupta, V.R.Subramanian. *ACS Omega*, **6**, 8734 (2021); https://doi.org/10.1021/ACSOMEGA.0C06045
223. S.Pei, H.M.Cheng. *Carbon*, **50**, 3210 (2012); https://doi.org/10.1016/j.carbon.2011.11.010
224. X.Li, B.Sun, Q.Wu, H.Fan, X.Liu, J.Cao, L.Yang, H.Liu, M.Wei. *J. Alloys Compd.*, **940**, 168796 (2023); https://doi.org/10.1016/J.JALLCOM.2023.168796
225. Y.Sheng, W.Li, L.Xu, Y.Zhu. *Adv. Mater.*, **34**, 2102354 (2022); https://doi.org/10.1002/ADMA.202102354
226. J.Wu, Y.Zhang, P.Lu, G.Fang, X.Li, W.W.Yu, Z.Zhang, B.Dong. *Appl. Catal. B: Environ.*, **286**, 119944 (2021); https://doi.org/10.1016/J.APCATB.2021.119944
227. A.Bafaqeer, M.Tahir, N.A.S.Amin, A.C.Ummer, H.A.Thabit, D.Dhamodharan, S.Ahmed, N.Kumar. *J. Alloys Compd.*, **968**, 171833 (2023); https://doi.org/10.1016/J.JALLCOM.2023.171833
228. D.Zhou, J.Zhang, Z.Jin, T.Di, T.Wang. *Chem. Eng. J.*, **450**, 138108 (2022); https://doi.org/10.1016/J.CEJ.2022.138108
229. Y.Yang, J.Wu, T.Xiao, Z.Tang, J.Shen, H.Li, Y.Zhou, Z.Zou. *Appl. Catal. B: Environ.*, **255**, 117771 (2019); https://doi.org/10.1016/J.APCATB.2019.117771
230. M.Gao, L.Sun, C.Ma, X.Li, H.Jiang, D.Shen, H.Wang, P.Huo. *Inorg. Chem.*, **60**, 1755 (2021); https://doi.org/10.1021/ACS.INORGCHEM.0C03233
231. X.Hu, J.Hu, Q.Peng, X.Ma, S.Dong, H.Wang. *Mater. Res. Bull.*, **122**, 110682 (2020); https://doi.org/10.1016/J.MATERRESBULL.2019.110682
232. A.Bafaqeer, M.Tahir, A.A.Khan, N.A.S.Amin. *Ind. Eng. Chem. Res.*, **58**, 8612 (2019); https://doi.org/10.1021/ACS.IECR.8B06053
233. X.Bian, S.Zhang, Y.Zhao, R.Shi, T.Zhang. *InfoMat*, **3**, 719 (2021); https://doi.org/10.1002/INF2.12192
234. L.Mohapatra, K.Parida. *J. Mater. Chem. A*, **4**, 10744 (2016); https://doi.org/10.1039/C6TA01668E
235. V.P.Tolstoy, L.B.Gulina, A.Meleshko. *Russ. Chem. Rev.*, **92** (3), RCR5071 (2023); https://doi.org/10.57634/RCR5071